Bond-length distributions for ions bonded to oxygen: Results for the lanthanides and actinides and discussion of the f-block contraction

Olivier Charles Gagné[a]*

[a]Geological Sciences, University of Manitoba, 125 Dysart Road, Winnipeg, Manitoba, R3T 2N2, Canada

Correspondence email: umgagneo@myumanitoba.ca

Synopsis Bond-length distributions have been examined for eighty-four configurations of the lanthanide ions and twenty-two configurations of the actinide ions bonded to oxygen. The lanthanide contraction for the trivalent lanthanide ions bonded to O^{2-} is shown to vary as a function of coordination number and to diminish in scale with increasing coordination number.

Abstract Bond-length distributions have been examined for eighty-four configurations of the lanthanide ions and twenty-two configurations of the actinide ions bonded to oxygen, for 1317 coordination polyhedra and 10,700 bond distances for the lanthanide ions, and 671 coordination polyhedra and 4754 bond distances for the actinide ions. A linear correlation between mean bond-length and coordination number is observed for the trivalent lanthanides ions bonded to O^{2-}. The lanthanide contraction for the trivalent lanthanide ions bonded to O^{2-} is shown to vary as a function of coordination number, and to diminish in scale with an increasing coordination number. The decrease in mean bond-length from La^{3+} to Lu^{3+} is 0.25 Å for CN 6 (9.8%), 0.22 Å for CN 7 (8.7%), 0.21 Å for CN 8 (8.0%), 0.21 Å for CN 9 (8.2%) and 0.18 Å for CN 10 (6.9%). The crystal chemistry of Np^{5+} and Np^{6+} is shown to be very similar to that of U^{6+} when bonded to O^{2-}, but differs for Np^{7+}.

Keywords: bond lengths; lanthanides; actinides; f-block; rare earth elements; lanthanide contraction; oxides; oxysalts.

1. Introduction

Comprehensive bond-length dispersion analyses done in the late 1980s (*e.g.*, Allen *et al.*, 1987; Mayer, 1988; Orpen *et al.*, 1989) have played a pivotal role in the fields of organic and organometallic chemistry. These works are useful in setting expectations and limits as to what bond lengths may be observed between ion pairs, and more generally serve as a distillation of crystallographic knowledge. However, this fundamental knowledge is lacking for inorganic compounds. A number of bond-length dispersion studies have been done since the 1970s for inorganic compounds, but have been limited to specific ions pairs; they are summarized in the first paper of this series (Gagné & Hawthorne, 2016). It is the goal of this series to provide a comprehensive description of bond lengths in inorganic compounds, and to provide easy access to a wealth of high-quality structural data for inorganic crystals for further studies. For a more detailed introduction and rationale for this work, as well as the description of the data-collection and data-filtering methods, see Gagné & Hawthorne (2015, 2016).

As part of our larger work on bond-length dispersion analysis, we have examined the distribution of bond lengths for 135 ions bonded to oxygen in 462 configurations using 180,331 bond lengths from 9367 refined crystal structures. These data cover most ions of the periodic table and all coordination numbers in which they occur where bonded to O^{2-}. Here, we report the bond-length distributions for 17 lanthanide and 9 actinide ions bonded to O^{2-}: 84 configurations of the lanthanide ions as a function of coordination number (n = 10,700 bond lengths and 1317 coordination polyhedra from 992 crystal structure refinements), and 22 configurations for the actinide ions (4754 bond lengths and 671 coordination polyhedra from 391 crystal-structure refinements). This paper is fourth in a series on the bond-length distributions of ions bonded to oxygen; other works in this series have analyzed bond lengths for the alkali and alkaline-earth metals bonded to O^{2-} (Gagné & Hawthorne, 2016), for the non-metals bonded to O^{2-} (Gagné & Hawthorne, 2017a), and for the metalloids and post-transition metals bonded to O^{2-} (Gagné & Hawthorne, 2017b).

2. Sample size

To ensure the reliability of the data we report, we have studied the effect of sample size on bond-length distributions. The effects of sampling (*e.g.*, the presence of outliers, non-random sampling) was reported in the first paper of this series (Gagné & Hawthorne, 2016). The effect of sample size on mean bond-length (and its standard deviation), skewness, and kurtosis were reported for $^{[6]}Na^{+}$ bonded to O^{2-}, for $^{[4]}S^{6+}$ and $^{[6]}I^{5+}$ bonded to O^{2-} and for $^{[4]}Si^{4+}$ and $^{[8]}Bi^{3+}$ bonded to O^{2-} in the first, second and third papers of this series, respectively (Gagné & Hawthorne, 2016, 2017a, 2017b). Gagné & Hawthorne (2017a) showed dependence of mean bond-length, skewness and kurtosis values on (1) number of data, (2) mean bond-valence, and (3) multi-modality of the bond-length distribution. Here, we analyze the effect of sample size on $^{[8]}La^{3+}$. The mean bond-valence of 3/8 v.u. has been sampled

before for $^{[8]}Bi^{3+}$ (Gagné & Hawthorne, 2017), but lone-pair stereoactive electrons give $^{[8]}Bi^{3+}$ a bimodal distribution of bond lengths, hence a possibly different dependence of some the parameters cited above as a function of sample size.

Fig. 1 shows that for $^{[8]}La^{3+}$, variation of less than ±0.005 Å in mean bond-length is observed for sample sizes of ~20 coordination polyhedra or more, while reliable values of skewness (±0.2) and kurtosis (±0.6) are obtained for sample sizes of 30 coordination polyhedra or more. In comparison, $^{[8]}Bi^{3+}$ (with stereoactive lone-pair electrons) gave analogous minimum sample sizes of 70 coordination polyhedra for mean bond-length, and 7 coordination polyhedra for skewness and kurtosis. Similarly, $^{[6]}I^{5+}$ (also bimodal with stereoactive lone-pair electrons) gave analogous minimum sample sizes of 40 coordination polyhedra for mean bond-lengths, while as little as 2 coordination polyhedra are enough to give reliable values of skewness and kurtosis. These results clearly show the effect of multi-modality; this is taken into consideration when reporting values of skewness and kurtosis for actinides with multi-modal behaviour (below).

For the description of mean-bond-length distributions, minimum sample sizes were determined for skewness and kurtosis with the same cut-offs as above, less than which these values have little significance and are not given. For $^{[8]}La^{3+}$, the threshold was observed at ~60 coordination polyhedra, although this value may in reality be higher but is limited here by the size of the parent distribution (n = 78). For multi-modal ions ($^{[6]}I^{5+}$, Gagné & Hawthorne, 2017a; $^{[8]}Bi^{3+}$, Gagné & Hawthorne, 2017b), the threshold observed for mean-bond-length distributions were ~65 and ~60 coordination polyhedra, respectively; this is also taken into consideration for reporting values of skewness and kurtosis below.

3. f-block contraction

The “f-block contraction”, used here as a unifying term to describe both the lanthanide and actinide contractions, dates back to Goldschmidt (1925) who coined the term “lanthanide contraction” following his observation of the decreasing size of these ions with an increasing atomic number.

The f-block contraction results from a shell-structure effect, where the incomplete shielding of the nuclear charge by the 4f (5f) electrons leads to the 6s (7s) electrons being drawn closer to the nucleus for these ions (Bagus, 1975). This effect increases with increasing nuclear charge along the series, and also accounts for the “d-block contraction” of the transition metals.

While shell-structure effects have a large role in the f-block contraction, a non-negligible component of the contraction is accounted for by the “relativistic effect”. The relativistic effect is explained by the relativistic mass increase of the electron for speeds nearing the speed of light which results in a reduction of the Bohr radius. While this effect primarily affects inner electrons (s and p shells), orthogonality constraints carry this effect to the shells of higher periods, similarly resulting in their contraction. In his review of relativistic effects in structural chemistry, Pyykkö (1988) attributes

roughly 10% of the lanthanide contraction to the relativistic effect, based on calculations of said contraction with and without the input of relativistic terms. Pyykkö states that the scale of the relativistic effect is comparable to that of structure-shell effects for period 6 (*i.e.*, lanthanides), but are more important for the actinides. Seth *et al.* (1995) showed that the actinide contraction is indeed primarily caused by the relativistic effect. The effect increases with group number in the periodic table and reaches its maximum for group 11 (Seth *et al.*, 1995).

The observed decrease in ionic radius for the lanthanides, from La^{3+} to Lu^{3+} (for coordination number 8), is 0.183 Å (Shannon, 1976). For the actinides, Ac^{3+} to Lr^{3+}, Pyykkö (1988) estimates the contraction at roughly 0.30 Å. The contraction along the lanthanide series has been reported as quadratic by Quadrelli (2001); this was confirmed by Seitz *et al.* (2007) for an isostructural series of trivalent La-Lu complexes ($R^2 > 0.99$); they also showed that the relation may be derived theoretically from Slater's model of atomic shielding constants (1930). This was expanded by Raymond *et al.* (2010) using hydrogen-type wave-functions.

We verify these results below.

4. Results

4.1. Lanthanides

For lanthanide ions bonded to O^{2-}, the collection and filtering criteria described in Gagné & Hawthorne (2016) resulted in a sample set of 10,700 bond lengths and 1317 coordination polyhedra.

Table 1 gives the mean bond-length and standard deviation, the minimum and maximum bond-length (and range), the skewness and kurtosis (where justified by sample size), and the number of bonds and coordination polyhedra for the 84 configurations in which we observe the 17 lanthanide ions bonded to O^{2-}. All bond-length and bond-valence distributions (using the bond-valence parameters of Gagné & Hawthorne, 2015) are deposited in Figs. S1 and S2, respectively; bond-length distributions of adequate sample size (see above) are shown in Fig. 2.

As we have done in the previous articles of this series, we have examined the data at the lower and upper limits of the bond-length distributions; these data are important in assigning a reliable range of bond lengths and bond valences that these ions may adopt. However, due to the regularity and similarity of the bond-length distributions for the lanthanide ions bonded to O^{2-}, *i.e.*, the absence of structural or electronic effects, a detailed discussion of the bonding behaviour of individual lanthanide ions is omitted. We discuss some general statistics for these ions below.

4.1.1. Coordination number

The lanthanides show a wide range in coordination number, generally from [6] to [12] (Table 1), and the variation is very systematic with atomic number. For the trivalent lanthanides, the dominant

coordination number is [8] followed by [9] for the light lanthanides (La, Ce, Nd, Eu, Gd, Tb) whereas it is [8] followed by [7] for the heavy lanthanides (Dy, Ho, Er, Ho, Er, Tm, Yb, Lu). Coordination number [6] is uncommon or absent for the light lanthanides, but becomes more significant for the heavy lanthanides (*e.g.*, Yb, Lu). For the tetravalent lanthanide ions, Ce is [8] followed by [9] whereas Tb is [6] only.

4.1.2. Mean bond-lengths

Fig. 3 shows the variation in grand mean bond-length as a function of coordination number for the trivalent lanthanides ions bonded to O^{2-} for sample sizes ≥ 10 coordination polyhedra. Only ions for which this resulted in 4 or more data points are shown for clarity. The correlation is linear, as was observed by Gagné & Hawthorne (2016) for the alkali- and alkaline-earth-metal ions bonded to O^{2-}. It is apparent from this plot that ions of higher atomic number progressively have shorter mean bond-lengths; this will be discussed in more detail below (see: *Observed f-block contraction for cations bonded to* O^{2-}).

We note that the slope of these correlations vary as a function of the size of the ion. For example, the slope for Er^{3+} in Fig. 3 is 5.29 x10^{-2} Å CN^{-1} and that of the larger La^{3+} ion 3.95 x10^{-2} Å CN^{-1}. This was also observed for the alkali and alkaline-earth metals bonded to O^{2-} (Fig. 7*a* in Gagné & Hawthorne, 2016), to a larger extent due to the relative difference in size of these ions (slopes of 0.119 Å CN^{-1} for Li^{+} and 3.86 x10^{-2} Å CN^{-1} for Cs^{+}). It is likely that this phenomenon arises from the relatively large difference in size for the different cations in relation to a relatively constant size for O^{2-}; the larger the cation, the less anion-anion repulsion there is for the same cation coordination number. For small cations, anion-anion repulsion results in distortion of the cation coordination polyhedron (*e.g.*, the radial expansion of bonds), an effect that increases with the number of bonds made to O^{2-}.

4.1.3. Skewness and kurtosis

Gagné & Hawthorne (2016) reported an inverse correlation between values of skewness and kurtosis of the bond-length distributions and coordination number for the alkali and alkaline-earth metal ions bonded to O^{2-}. We do not observe such a clear-cut trend for the trivalent lanthanide ions, except for coordination number [7], where a positive correlation between the skewness and kurtosis of the bond-length distributions is observed with the number of f electrons of the ions. Fig. 4 gives (*a*) skewness and (*b*) kurtosis of the bond-length distribution as a function of the number of f electrons. When removing data points that account for less than 10 coordination polyhedra, R^2 decreases from 0.65 to 0.63, but kurtosis increases from 0.53 to 0.81. The reasons behind the positive correlation are unclear; it is possible that this is caused by inadequate sample size, as the mean sample size in Fig. 4 is 16 coordination polyhedra.

4.1.4. Bond-length range

There are too few data for these ions to observe any meaningful trend in bond-length ranges as a function of coordination number. Generally, the ranges in individual bond-lengths increase with coordination number (Table 1). Where this does not occur, *e.g.*, for [11]-coordination for La^{3+} or [10]-coordination for Er^{3+} (Table 1), it is commonly associated with a very small number of coordination polyhedra.

4.2. Actinides

For the actinide ions bonded to O^{2-}, the collection and filtering criteria described in Gagné & Hawthorne (2016) resulted in a sample size of 4754 bonds and 671 coordination polyhedra. Table 2 gives the mean bond-length and standard deviation, the minimum and maximum bond-length (and range), the skewness and kurtosis (where justified by sample size), and the number of bonds and coordination polyhedra for the 22 configurations in which we observe the 9 actinide ions bonded to O^{2-}. All bond-length and bond-valence distributions are deposited in Figs. S3 and S4, respectively; bond-length distributions of adequate sample size are shown in Fig. 5.

As for the lanthanides, we have examined the data at the lower and upper limits of the bond-length distributions for the actinides bonded to O^{2-}. However, the sample size for these ions are limited (aside from U^{6+}), thus we leave out the statistical analysis of these ions. A discussion of the crystal-chemistry of actinide ions with multi-modal bond-length distributions is given below.

5. Discussion

5.1. Mean bond-length distributions

The mean bond-length distributions for the lanthanide and actinide ions bonded to O^{2-} are given in Figs. S5 and S6, respectively; those with adequate sample size (see sample-size study above) are given in Figs. 6 and 7. Tables 3 and 4 give the grand mean-bond-length and standard deviation, the minimum and maximum mean bond-lengths (and range), the skewness and kurtosis of each distribution (where justified by sample size), and the number of coordination polyhedra and coordination numbers for all configurations observed.

For the ion configurations of lanthanides bonded to O^{2-}, the average range of mean bond-lengths observed is 0.096 Å for sample sizes greater than 10 coordination polyhedra; for the actinide ions, this range is 0.067 Å. Although we deal with much fewer data here, mean bond-length ranges for these families are comparable to that of the strongly-bonded oxyanions (*e.g.*, S^{6+} = 0.063 Å, C^{4+} = 0.078 Å, Si^{4+} = 0.092 Å, N^{5+} = 0.100 Å; Gagné & Hawthorne 2017a,b). In comparison, the observed range of mean bond-lengths observed for alkali and alkaline-earth metals bonded to O^{2-} are typically ~0.3-0.4 Å and ~0.20-0.25 Å (Gagné & Hawthorne, 2016), respectively, and ~0.1-0.3 Å for ions with stereoactive lone-pair electrons (Gagné & Hawthorne, 2017a,b).

We give the bond-length distortion plots for the lanthanide and actinide ions bonded to O^{2-} in Figs. S7 and S8, and in Figs. 8 and 9 for those with adequate sample size. We use the definition of Brown and Shannon (1973) for distortion, *i.e.*, the mean-square relative deviation of bond lengths from their average value. Despite being only weakly distorted where the polyhedra are not regular (distortion < 10 x 10^{-3}), lanthanide ions show an unusually high correlation between mean bond-length and bond-length distortion (R^2 ~ 0.3-0.7); metalloid, post-transition metal and non-metal ions with bond-length distortion less than 10 x 10^{-3} are rarely observed with R^2 > 0.15. Actinide ions bonded to O^{2-} with sufficient data are typically observed as moderately distorted (~10-30 x 10^{-3}), and also show a strong correlation between mean bond-length and distortion (R^2 ~ 0.5-0.7). This follows the studies for H^+ and for ions with stereoactive lone-pair electrons of Gagné & Hawthorne (2017a,b), who reported that ion configurations with distortion values > 10-20 x 10^{-3} typically show a high correlation between mean bond-length and distortion.

A thorough examination of potential factors leading to mean bond-length variation was done by Gagné & Hawthorne (2017c) for 55 ion configurations bonded to O^{2-}. Unfortunately, limitations of sample size made lanthanide ions bonded to O^{2-} unsuitable for their analysis; however, $^{[7]}U^{6+}$ was analyzed (n = 69 coordination polyhedra). For $^{[7]}U^{6+}$, Student *t*-tests showed that for (1) bond-length distortion, (2) mean coordination-number of the bonded anions, (3) mean electronegativity, and (4) mean ionization energy of the next-nearest neighbours, only bond-length distortion is significantly correlated with mean bond-length for the 95% confidence level (*p*-value = 9.6 x 10^{-4}). This gives R^2 = 0.15 for their sample of $^{[7]}U^{6+}$, which is significantly different than that of the parent population (Fig. 9*b*; R^2 = 0.46, n = 448). These results clearly show the effect of sample size on these types of correlations, and this was studied by Gagné & Hawthorne (2017c) who showed that both *p*-values and R^2 values vary significantly as a function of sample size for samples smaller than 100 coordination polyhedra. While a R^2 value ~0.3 *below* that of the parent population was obtained in this particular case, the occurrence of false positives seems likely where dealing with sample sizes of less than 100 coordination polyhedra. This is one argument that Gagné & Hawthorne (2017c) use to show that contrary to common usage, published correlations between mean bond-length and the mean coordination number of the bonded anions are not of general applicability to inorganic oxide and oxysalt structures; early studies that suggested this correlation may have been affected by small sample size.

As discussed above, it is clear from Figs. 8 and 9 that mean bond-length is highly correlated with bond-length distortion for the lanthanide and actinide ions bonded to O^{2-}; this is further supported by the distortion theorem (*e.g.*, Brown & Shannon, 1973; Allmann, 1975; Brown, 1978; Urusov, 2003) which proves causality for this relation. However, with R^2 = 0.15 for $^{[7]}U^{6+}$, it is clear that other factors are present and of greater importance. Gagné & Hawthorne (2017c) proposed that the inability of crystal structures to attain their ideal (*a priori*) bond-lengths within the constraints of space-group

symmetry is likely the leading cause of mean bond-length variation in crystals, citing examples for $^{[3]}Al^{3+}$, $^{[6]}Al^{3+}$ and $^{[12]}Ba^{2+}$. However, they state that a clear and reliable way to quantify the stress produced by the inability of a structure to follow its a *priori* bond-lengths remains to be established.

5.2. Bond-valence sums

Although there should be no correlation between incident bond-valence sum and coordination number, Gagné & Hawthorne (2016) found a positive correlation between mean bond-valence sum and coordination number for the alkali- and alkaline-earth-metals bonded to O^{2-}. This correlation was obtained despite using the bond-valence parameters of Gagné & Hawthorne (2015) who added a coordination-based optimization factor in the derivation of their bond-valence parameters to minimize this effect; other sets of published parameters give larger deviations. Due to their observation in a wide range of coordination number, the trivalent lanthanide ions are good candidates to see whether this effect is restricted to the alkali- and alkaline-earth-metals.

To do this, we calculate the mean slope (mean absolute slope) of the grand mean bond-valence sum of the ions as a function of their coordination number using the parameters of Gagné & Hawthorne (2015). For the 14 trivalent lanthanide ions, the mean slope is 5.5×10^{-3} (1.3×10^{-3}). In comparison, the bond-valence parameters of Brese & O'Keeffe (1991) give a mean slope of -5.2×10^{-2} (5.1×10^{-2}), and those of Brown & Altermatt (1985) -3.5×10^{-2} (4.0×10^{-2}). Thus the parameters of Gagné & Hawthorne (2015) are more consistent with the valence-sum rule than other published sets of bond-valence parameters, and are especially suited for ions that occur in multiple coordination numbers as they give a mean slope closer to zero. The mean slope obtained from the data of Gagné & Hawthorne (2016), using the parameters of Gagné & Hawthorne (2015), is 1.8×10^{-2} for the alkali metals and 1.6×10^{-2} for the alkaline-earth metals bonded to O^{2-}, indicating that the correlation between bond-valence sum and coordination number is more important for the alkali and alkaline-earth metals.

It is possible that the difficulty of the bond-valence model to give accurate bond-valence sums for the unusually low and high coordination numbers of certain cations results from the argument of anion-anion repulsion described above.

5.3. Bond-length distributions for lanthanide ions bonded to O^{2-}

The lanthanide ions display fairly consistent behaviour across the series when bonded to O^{2-} (Fig. 2). This is due to the largely electrostatic nature of the chemical bonds they form (Neidig *et al.*, 2013) as the 4f electrons of these ions have been shown not to participate in bonding (Maron & Eisenstein, 2000; Choppin, 2002). However, we observe a number of coordination polyhedra in our dataset with one or two bonds to O^{2-} that appear to be anomalously long. For example, the sixth and seventh shortest interatomic distances are 2.371 and 2.635 Å for 7-coordinated Yb^{3+} in $Li_2Yb_5O_4(BO_3)_3$ (Jubera *et al.*, 2001), and the bond-length 2.635 Å appears to fall outside of the main distribution of

bond lengths for $^{[7]}Yb^{3+}$ (Fig. 2*ai*). Structures where this occurs are typically borates, and otherwise host ions with lone-pair stereoactive electrons; the occurrence of these long bonds may be the result of designed synthetic efforts.

5.4. Multi-modal bond-length distributions for actinide ions bonded to O^{2-}: crystal chemistry of U and Np

Some actinides are well known to form actinyl ions with oxygen, $(AnO_2)^{n+}$. These complexes have short and strong An-O bonds, and form weaker bonds to ligands in their equatorial plane, leading to typical An coordination numbers of [6] to [8]. The more common actinyl ions include the uranyl ($[U^{6+}O_2]^{2+}$), neptunyl ($[Np^{5+}O_2]^{+}$, $[Np^{6+}O_2]^{2+}$) and plutonyl ($[Pu^{6+}O_2]^{2+}$) oxycations. These ions form from the mixing of oxygen p orbitals and actinide empty d and empty (U) or partially-occupied (Np, Pu) f orbitals (Craw *et al.*, 1995; Denning, 2007), where in the latter case the f electrons reside in δ_u orbitals which do not overlap with oxygen orbitals. The uranyl ion is well studied due to the abundance and technological importance of U. For a detailed description of the crystal chemistry of U^{6+} bonded to O^{2-}, we refer the reader to Burns *et al.* (1997); for other ligands, see Hayton (2010).

In our bond-length dispersion analysis, we observe the following actinyl oxycations: $(U^{6+}O_2)^{2+}$, $(Np^{5+}O_2)^{+}$ and $(Np^{6+}O_2)^{2+}$. The $(U^{6+}O_2)^{2+}$ and $(Np^{5+}O_2)^{+}$ complexes occur with 4, 5 and 6 equatorial bonds to other O^{2-} ions; $(Np^{6+}O_2)^{2+}$ is observed with 5 and 6 equatorial bonds. Structures with U^{6+} in coordination number [6] do not always form the uranyl ion; 7 of 94 $U^{6+}O_6$ coordination polyhedra in our dataset are regular octahedra, and all are synthetics. The bond-length distribution of $^{[6]}U^{6+}$ (Fig. 5*e*) appears to be tri-modal as a result of this, whereby the bond-length distribution of the regular $U^{6+}O_6$ octahedra forms a small distribution of bonds between that of the $U\text{-}O_{uranyl}$ and $U\text{-}O_{equatorial}$ bonds in square-bipyramidal geometry. These bond lengths range from 2.05-2.09 Å, and examination of the bond-valence distribution for $^{[6]}U^{6+}$ (Fig. S4*l*) shows that this corresponds to a mean bond-valence of ~1 v.u. Thus the two bins at these distances in Fig. 5*e* are explained by structures which form regular $U^{6+}O_6$ octahedra. More details of the crystal chemistry and coordination geometry of U^{6+} bonded to O^{2-} can be seen in Burns *et al.* (1997); however, we make two small additions to this work. First, we observe a correlation between the mean $(U^{6+}O_2)^{2+}$ bond length and coordination number, albeit subtle: the mean bond-lengths of the uranyl complex are 1.798 Å, 1.791 Å and 1.781 Å for coordination numbers [6], [7] and [8], respectively (1.690, 1.716 and 1.753 v.u. using the bond-valence parameters of Gagné & Hawthorne, 2015). Second, the bond-length distribution of $^{[8]}U^{6+}$ bonded to O^{2-} (Fig. 5*g*) may be split into those structures where $^{[8]}U^{6+}$ is observed in [2+2+4]- and [2+6]-coordination. This is shown in Fig. 10; the bond-length distribution for the subset of [2+2+4] structures consisting of roubaultite (Ginderow & Cesbron, 1985),$Cu_2(UO_2)_3(CO_3)_2O_2(OH)_2(H_2O)_4$, dumonite (Piret & Piret-Meunier, 1988), $Pb_2((UO_2)_3O_2(PO_4)_2)(H_2O)_5$, marthozite (Cooper & Hawthorne, 2001),$Cu((UO_2)_3(SeO_3)_2O_2)(H_2O)_8$, bergenite (Locock & Burns, 2003a),

$Ca_2(Ba_{3.69}Ca_{0.31})((UO_2)_3O_2(PO_4)_2)_3(H_2O)_{16}$ and huegelite (Locock & Burns, 2003b), $Pb_2(UO_2)_3O_2(AsO_4)_2(H_2O)_5$ is given in Fig. 10*a*, and that of the much larger subset of [2+6] structures is given in Fig. 10*b*, which together give Fig. 10*c*.

The crystal chemistry of Np^{5+} and Np^{6+} appears to be very similar to that of U^{6+}; these ions also form actinyl complex with 4 to 6 bonds in their equatorial plane. The bond-length distributions for the various coordination numbers of these ions appear to be simpler and more regular than those of U^{6+}, although this may be due to much smaller sample sizes (31, 7 and 585 coordination polyhedra for Np^{5+}, Np^{6+} and U^{6+}, respectively). Thus we do not observe symmetrical configuration of the Np^{5+} and Np^{6+} ions in coordination number [6] in our dataset, and do not observe an evident deviation from [2+6]-coordination for coordination number [8] for these ions. For Np^{5+}, the mean bond-length for the actinyl ion and the equatorial bonds (mean bond-valence using the parameters of Gagné & Hawthorne, 2015) are (Å): [6] 1.845 (1.591 v.u.), 2.394 (0.418 v.u.), [7] 1.838 (1.619 v.u.), 2.461 (0.355 v.u.) with bond-length range 2.360-2.591, and [8] 1.845 (1.591 v.u.), 2.544 (0.290 v.u.) with bond-length range 2.352-2.770. For Np^{6+}, the corresponding values are: [7] 1.744 (1.701 v.u.), 2.367 (0.517 v.u.) with bond-length range 2.297-2.486, and [8] 1.773 (1.609 v.u.) and 2.424 (0.463 v.u.). Like U^{6+}, both ions have a strong preference for pentagonal-bipyramidal coordination [7], which is the configuration for 84% and 86% of observed polyhedra for Np^{5+} and Np^{6+}, respectively (76% for U^{6+}). These numbers may vary as more data are collected.

On the other hand, Np^{7+} forms strongly-bonded $(Np^{7+}O_4)^-$ oxyanions in square-planar coordination. These complexes make two longer bonds to oxygen arranged at the apices of an elongated octahedron. There are only two examples of such structures in our data: $Co(NH_3)_6NpO_4(OH)2(H_2O)_2$ (Grigor'ev *et al.*, 1986), and $Cs_3(NpO_4(OH)_2)(H_2O)_3$ (Grigor'ev *et al.*, 1993). The mean bond-length of the 4 short and 2 long bonds are 1.892 and 2.362 Å, respectively (1.45 v.u. and 0.55 v.u. using the bond-valence parameters of Gagné & Hawthorne, 2015). The $Np^{7+}O_6$ octahedra do not polymerize in these structures.

5.5. Observed f-block contraction for cations bonded to O^{2-}

The ionic radii of Shannon (1976) suggest that the trivalent lanthanide ions contract by 0.183 Å from La^{3+} to Lu^{3+} for coordination number [8]; for the actinide contraction, Pyykkö (1988) suggested a corresponding contraction of 0.30 Å. As most actinide radii are not available from Shannon's set of ionic radii (1976), it is unclear how Pyykkö arrived at this value. However, Küchle *et al.* (1997) suggested a simple linear extrapolation of the radii of Ac^{3+} (1.12 Å) and Es^{3+} (0.94 Å), for which they assess the total actinide contraction to be in the range 0.22-0.25 Å.

The curvature of the lanthanide contraction for trivalent ions has been investigated by Quadrelli (2002), Seitz *et al.* (2007) and Raymond *et al.* (2010). Quadrelli (2002) gave the mean bond-length of the three equatorial bonds and that of the six other bonds as a function of the number of electrons in

the f shell for a series of isotypical compounds in which the lanthanide ions are [9]-coordinated. Seitz *et al.* (2007) gave the sum of all Ln-O bonds (Ln = lanthanide) as a function of the number of electrons in the f shell for a different series of isotypical compounds of the Ln ions with coordination number [8]. Raymond *et al.* (2010) gave the inverse of the ionic radius as a function of the number of f electrons in different lanthanide complexes and obtained a linear correlation. Our data show a nearly identical fit whether we plot mean bond-length or the inverse of ionic radius as a function of the number of f electrons; however, the relation of Raymond *et al.* (2010) has the advantage of being linear, while those of Quadrelli (2002) and Seitz *et al.* (2007) are quadratic.

Fig. 11 shows the inverse of the ionic radii of the trivalent lanthanide ions as a function of the number of f electrons. To calculate the ionic radii, we subtracted 1.38 Å from the mean bond-length; we do not list these radii to replace those of Shannon (1976) in the present work, as a more comprehensive derivation is in progress. We obtain a very good fit for coordination numbers [6] (R^2 = 0.979), [7] (R^2 = 0.988), [8] (R^2 = 0.982) and [9] (R^2 = 0.968), a borderline fit for coordination number [10] (R^2 = 0.779), and the correlation is lost for coordination numbers [11] and [12], possibly due to paucity of data. Very similar results are obtained using the crystal radius of Shannon (1976) and instead subtracting 1.24 Å from the mean bond-length. Whereas the studies reported above gave $R^2 > 0.99$ for isotypical compounds, the correlations we derive here are for a variety of structure types, thus have wider applicability. The equations for the different coordination numbers are: [6] 1.8 r_{Ln} x 10^{-2} + 0.948, [7] 1.44 r_{Ln} x 10^{-2} + 0.901, [8] 1.23 r_{Ln} x 10^{-2} + 0.874, [9] 1.2 r_{Ln} x 10^{-2} + 0.840 and [10] 9.3 r_{Ln} x 10^{-3} + 0.807. The slope of this relation decreases as the coordination number increases (Fig. 11), *i.e.*, the scale of the contraction diminishes with increasing coordination number. This follows the anion-anion repulsion argument described above. Seitz *et al.* (2007) report that for the lanthanides, individual bond-lengths decrease by approximately 7-8% from La to Lu (coordination number [8]). According to the best-fit equations given above for coordination numbers [6] to [10], the lanthanide contraction results in a decrease in mean bond-length from La^{3+} to Lu^{3+} of 0.25 Å for CN [6] (9.8%), 0.22 Å for CN [7] (8.7%), 0.21 Å for CN [8] (8.0%), 0.21 Å for CN [9] (8.2%) and 0.18 Å for CN [10] (6.9%).

Treatment of the actinide ions is complicated by the paucity of experimental data and the observation of these ions in multiple oxidation states; the collection criteria for our bond-length dispersion analysis have resulted in two trivalent (Am^{3+}, Cm^{3+}), tetravalent (Th^{4+}, U^{4+}), pentavalent (U^{5+}, Np^{5+}) and hexavalent (U^{6+} and Np^{6+}) ions, and one heptavalent ion (Np^{7+}). Extrapolation is prone to large error due to the isovalent ions typically being adjacent in the f-block, thus we do not extend this analysis to the actinide ions.

6. Summary

(1) We have examined the bond-length distributions for eighty-four configurations of the lanthanide ions bonded to O^{2-} using 1317 coordination polyhedra and 10,700 bond distances, and for twenty-two configurations of the actinide ions bonded to O^{2-} using 671 coordination polyhedra and 4754 bond distances.

(2) We observe a linear correlation between mean bond-length and coordination number for the trivalent lanthanides ions bonded to O^{2-}.

(3) We show that the correlation between the inverse of the ionic radius and the number of f electrons for the trivalent lanthanide ions bonded to O^{2-} holds across various structure types.

(4) We show that the lanthanide contraction for the trivalent lanthanide ions bonded to O^{2-} varies as a function of coordination number; this results in a decrease in mean bond-length from La^{3+} to Lu^{3+} of 0.25 Å for CN 6 (9.8%), 0.22 Å for CN 7 (8.7%), 0.21 Å for CN 8 (8.0%), 0.21 Å for CN 9 (8.2%) and 0.18 Å for CN 10 (6.9%). The lanthanide contraction diminishes in scale with an increasing coordination number, which follows an increase in anion-anion repulsion with increasing coordination number.

(5) We show that bond-length distortion is a major cause of mean-bond-length variation for the lanthanide and actinide ions bonded to O^{2-}. It is suspected that the largest cause of mean bond-length variation for these ions is the inability of crystal structures to attain their ideal (*a priori*) bond-lengths within the constraints of space-group symmetry.

(6) We show that using the bond-valence parameters of Gagné & Hawthorne (2015) removes most of the correlation between mean bond-valence sum and coordination number obtained using other sets of bond-valence parameters.

(7) When bonded to O^{2-}, the crystal chemistry of Np^{5+} and Np^{6+} appears to be very similar to that of U^{6+}. These ions form strongly-bonded actinyl ($[AnO_2]^{n+}$) oxycations with 4 to 6 bonds in their equatorial plane. On the other hand, Np^{7+} form a strongly-bonded $(Np^{7+}O_4)^{-}$ oxyanion in square-planar coordination with 2 longer bonds to O^{2-} at the apices of an elongated octahedron. An in depth-study of the crystal chemistry of Np^{7+} awaits collection of more data.

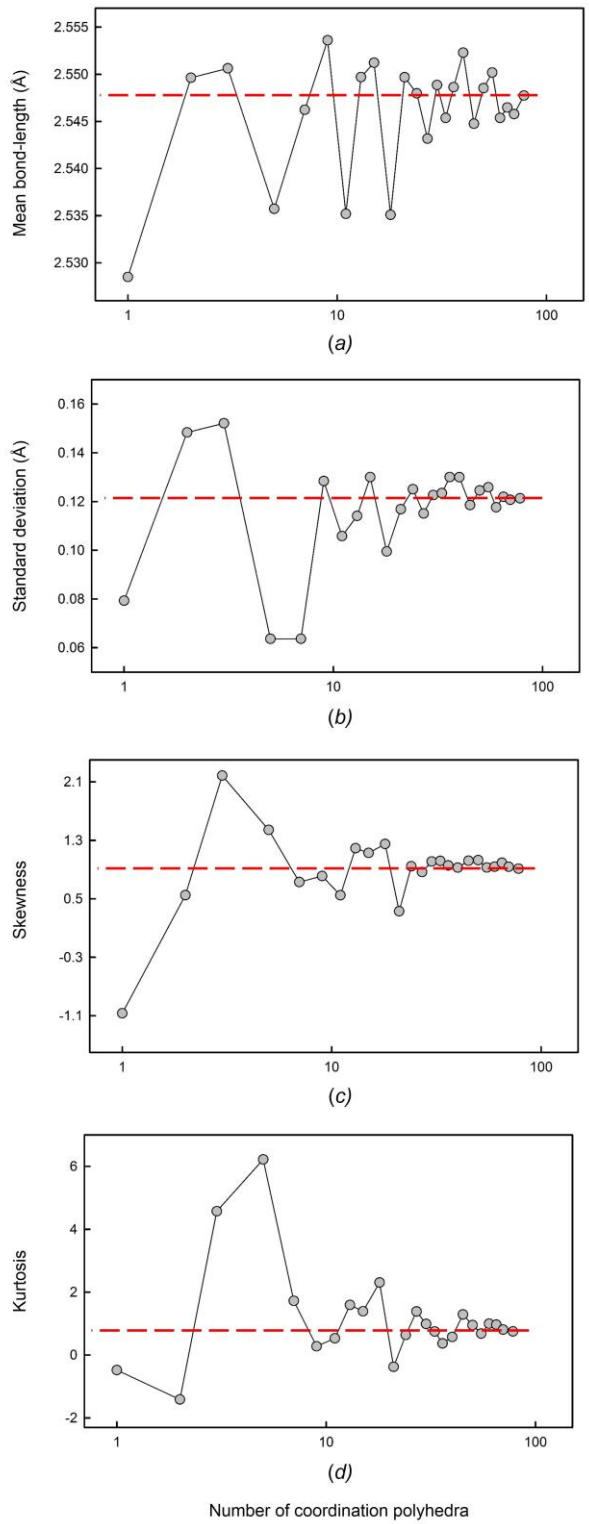

Figure 1 The effect of sample size on (*a*) skewness (*b*) kurtosis (*c*) mean bond-length, and (*d*) standard deviation of the mean bond-length for $^{[8]}La^{3+}$. The dashed line shows the value for the parent distribution.

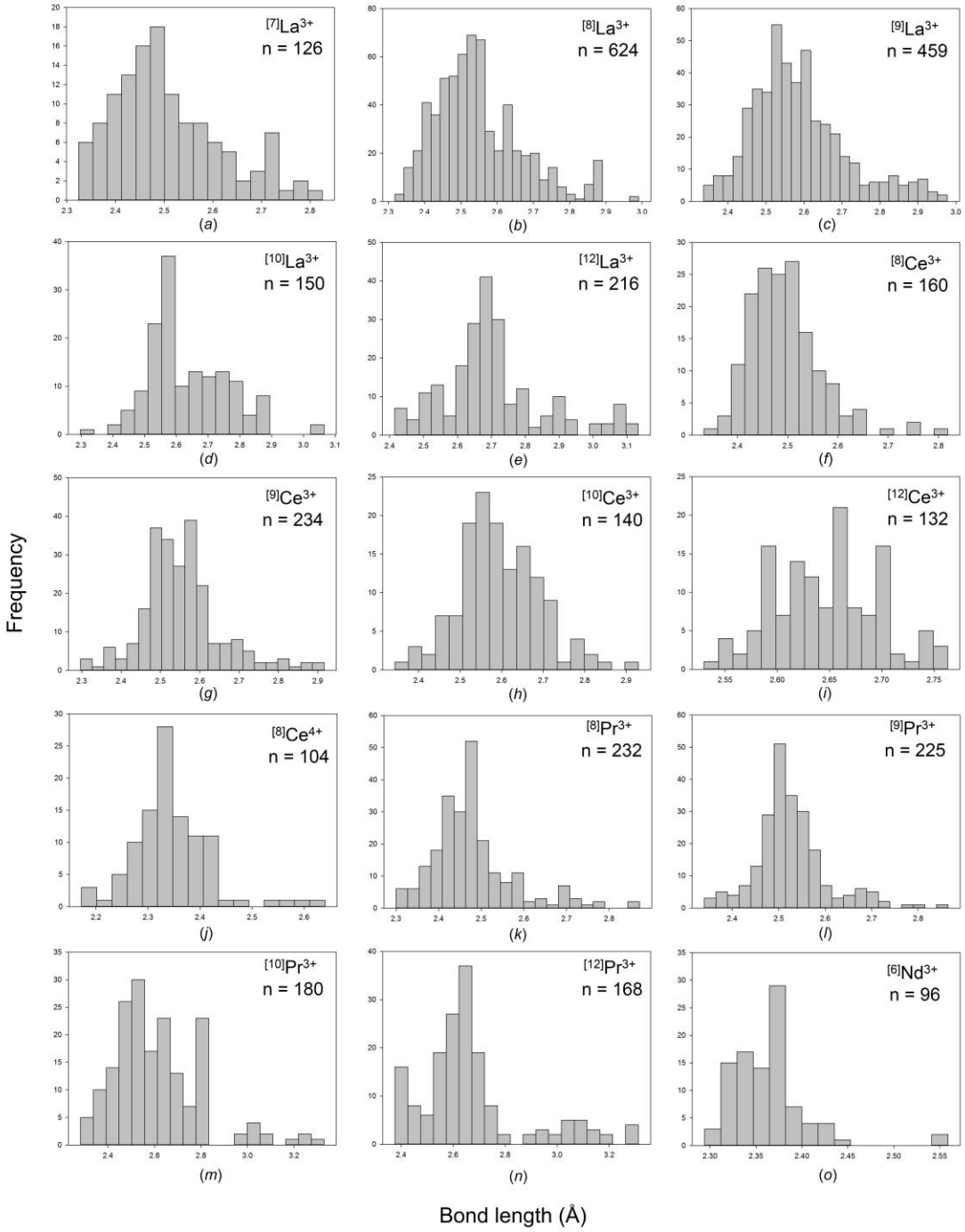
[7]La3+
n = 126
(a)
[8]La3+
n = 624
(b)
[9]La3+
n = 459
(c)
[10]La3+
n = 150
(d)
[12]La3+
n = 216
(e)
[8]Ce3+
n = 160
(f)
[9]Ce3+
n = 234
(g)
[10]Ce3+
n = 140
(h)
[12]Ce3+
n = 132
(i)
[8]Ce4+
n = 104
(j)
[8]Pr3+
n = 232
(k)
[9]Pr3+
n = 225
(l)
[10]Pr3+
n = 180
(m)
[12]Pr3+
n = 168
(n)
[6]Nd3+
n = 96
(o)
Frequency
Bond length (Å)

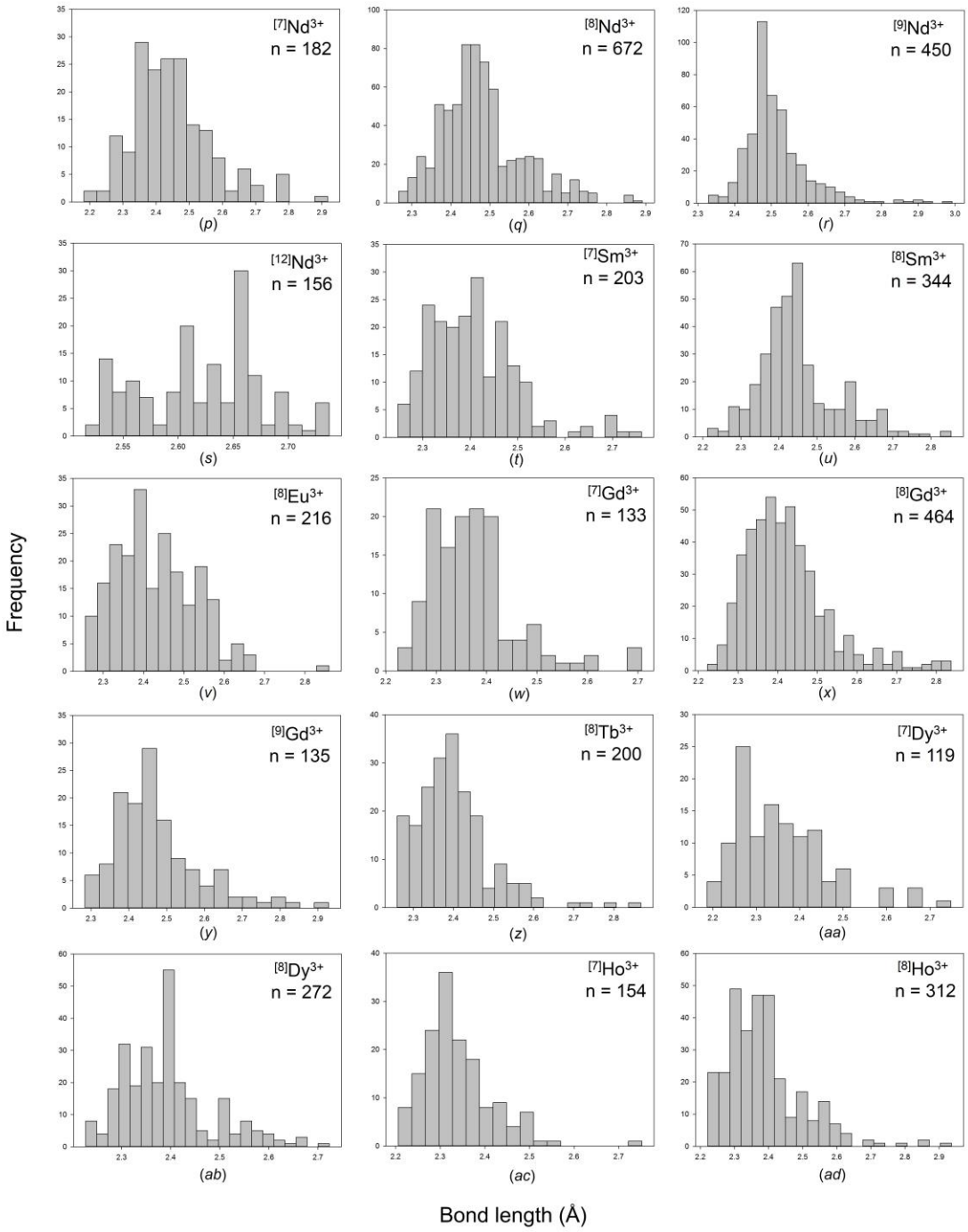
[7]Nd3+
n = 182
(p)
[8]Nd3+
n = 672
(q)
[9]Nd3+
n = 450
(r)
[12]Nd3+
n = 156
(s)
[7]Sm3+
n = 203
(t)
[8]Sm3+
n = 344
(u)
[8]Eu3+
n = 216
(v)
[7]Gd3+
n = 133
(w)
[8]Gd3+
n = 464
(x)
[9]Gd3+
n = 135
(y)
[8]Tb3+
n = 200
(z)
[7]Dy3+
n = 119
(aa)
[8]Dy3+
n = 272
(ab)
[7]Ho3+
n = 154
(ac)
[8]Ho3+
n = 312
(ad)
Frequency
Bond length (Å)

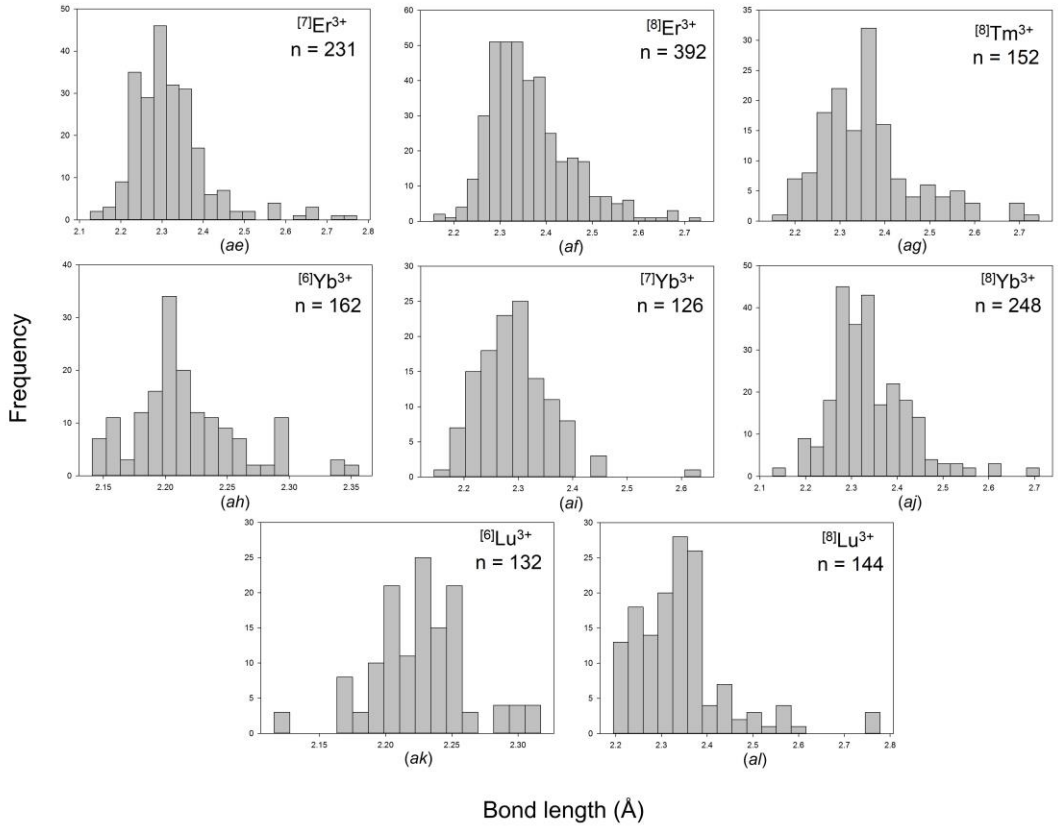

Figure 2 Bond-length distributions for selected configurations of the lanthanide ions bonded to O^{2-}: (*a*) $^{[7]}La^{3+}$, (*b*) $^{[8]}La^{3+}$, (*c*) $^{[9]}La^{3+}$, (*d*) $^{[10]}La^{3+}$, (*e*) $^{[12]}La^{3+}$, (*f*) $^{[8]}Ce^{3+}$, (*g*) $^{[9]}Ce^{3+}$, (*h*) $^{[10]}Ce^{3+}$, (*i*) $^{[12]}Ce^{3+}$, (*j*) $^{[8]}Ce^{4+}$, (*k*) $^{[8]}Pr^{3+}$, (*l*) $^{[9]}Pr^{3+}$, (*m*) $^{[10]}Pr^{3+}$, (*n*) $^{[12]}Pr^{3+}$, (*o*) $^{[6]}Nd^{3+}$, (*p*) $^{[7]}Nd^{3+}$, (*q*) $^{[8]}Nd^{3+}$, (*r*) $^{[9]}Nd^{3+}$, (*s*) $^{[12]}Nd^{3+}$, (*t*) $^{[7]}Sm^{3+}$, (*u*) $^{[8]}Sm^{3+}$, (*v*) $^{[8]}Eu^{3+}$, (*w*) $^{[7]}Gd^{3+}$, (*x*) $^{[8]}Gd^{3+}$, (*y*) $^{[9]}Gd^{3+}$, (*z*) $^{[8]}Tb^{3+}$, (*aa*) $^{[7]}Dy^{3+}$, (*ab*) $^{[8]}Dy^{3+}$, (*ac*) $^{[7]}Ho^{3+}$, (*ad*) $^{[8]}Ho^{3+}$, (*ae*) $^{[7]}Er^{3+}$, (*af*) $^{[8]}Er^{3+}$, (*ag*) $^{[8]}Tm^{3+}$, (*ah*) $^{[6]}Yb^{3+}$, (*ai*) $^{[7]}Yb^{3+}$, (*aj*) $^{[8]}Yb^{3+}$, (*ak*) $^{[6]}Lu^{3+}$, (*al*) $^{[8]}Lu^{3+}$.

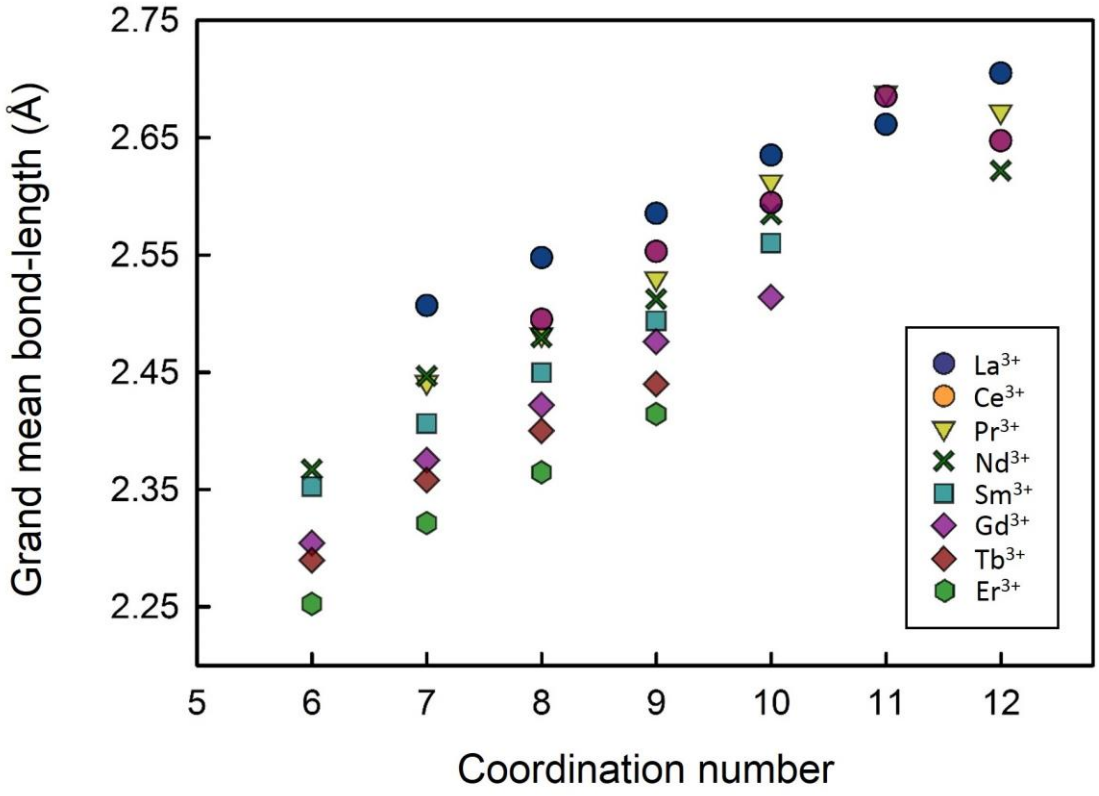

Figure 3 Mean bond-length as a function of coordination number for La^{3+}, Ce^{3+}, Pr^{3+}, Nd^{3+}, Sm^{3+}, Gd^{3+}, Tb^{3+} and Er^{3+} for sample sizes ≥ 5 coordination polyhedra.

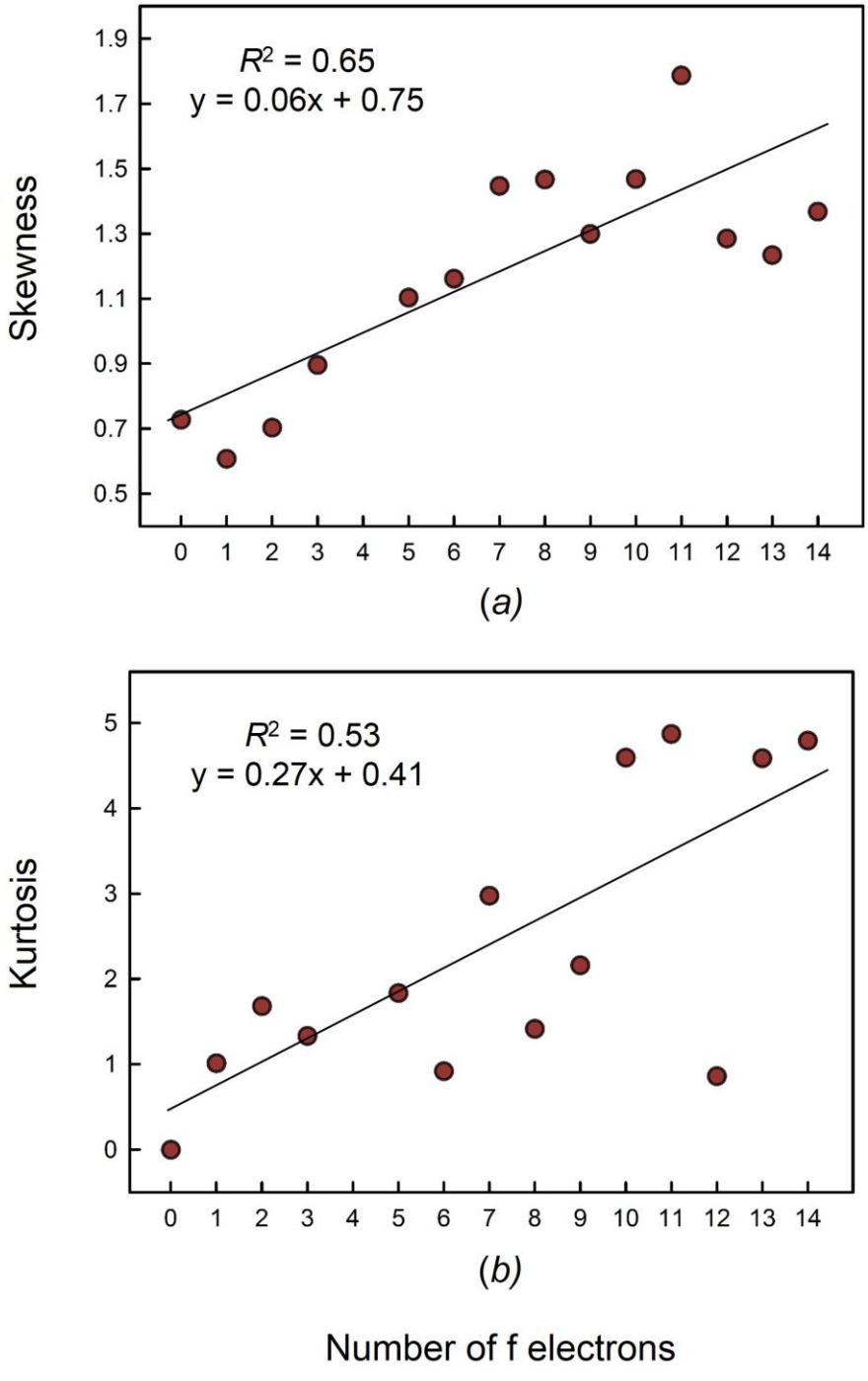

Figure 4 Correlation between (*a*) skewness and (*b*) kurtosis of the bond-length distribution as a function of the number of f electrons for coordination number 7 of the lanthanide ions.

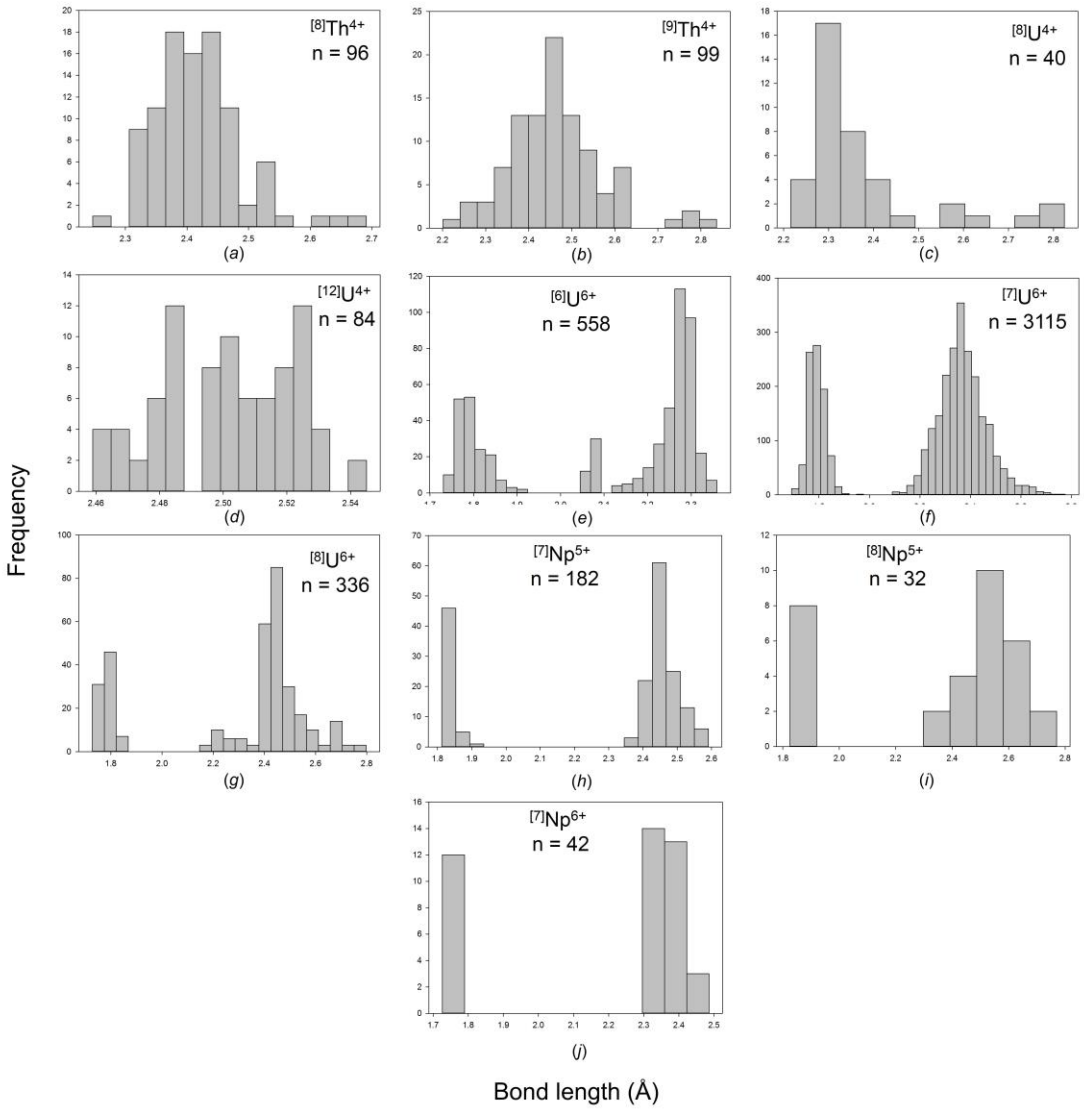

Figure 5 Bond-length distributions for selected configurations of the actinide ions bonded to O^{2-}: (*a*) $^{[8]}Th^{4+}$, (*b*) $^{[9]}Th^{4+}$, (*c*) $^{[8]}U^{4+}$, (*d*) $^{[12]}U^{4+}$, (*e*) $^{[6]}U^{6+}$, (*f*) $^{[7]}U^{6+}$, (*g*) $^{[8]}U^{6+}$, (*h*) $^{[7]}Np^{5+}$, (*i*) $^{[8]}Np^{5+}$, (*j*) $^{[7]}Np^{6+}$.

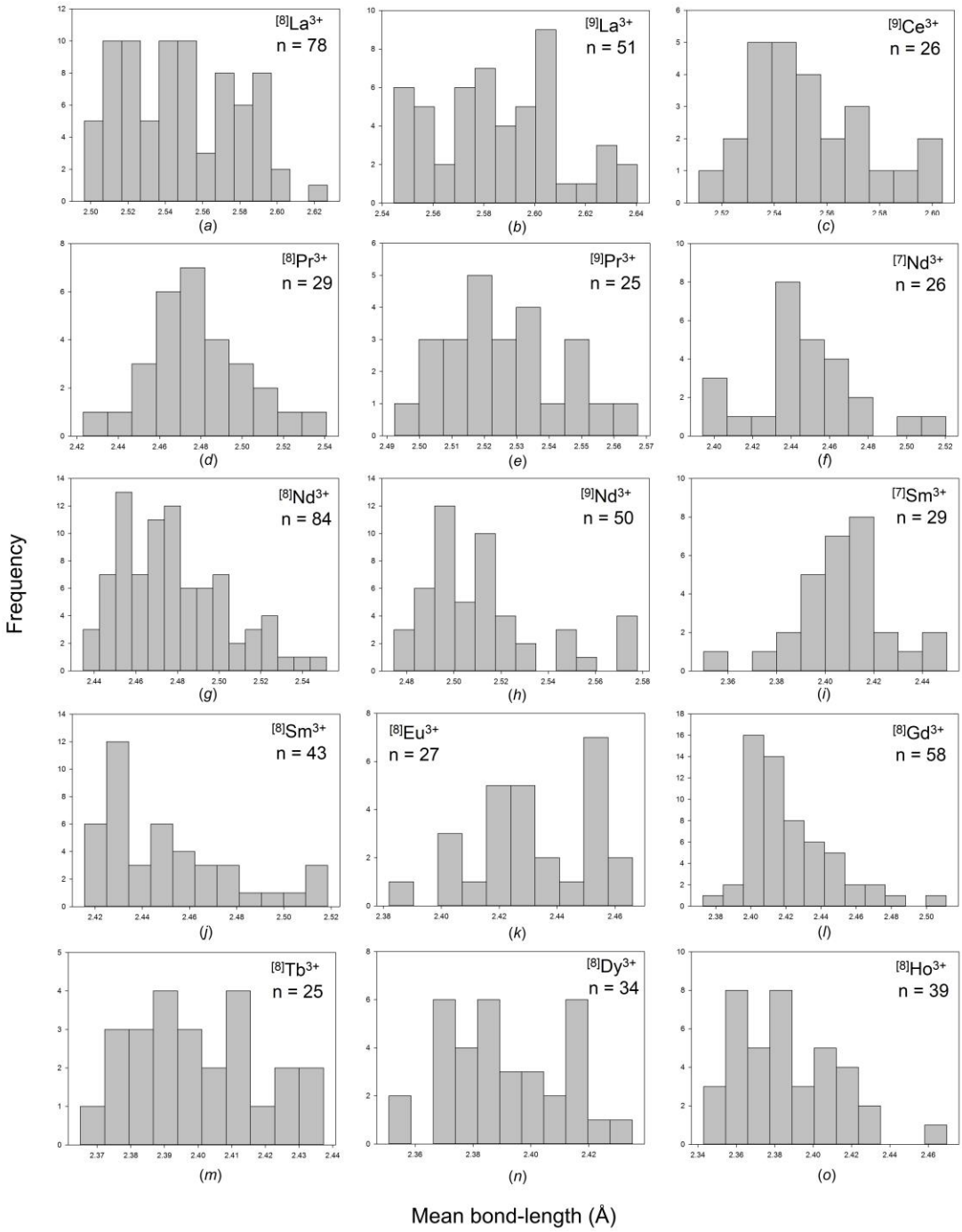
[8]La3+
n = 78
(a)
[9]La3+
n = 51
(b)
[9]Ce3+
n = 26
(c)
[8]Pr3+
n = 29
(d)
[9]Pr3+
n = 25
(e)
[7]Nd3+
n = 26
(f)
[8]Nd3+
n = 84
(g)
[9]Nd3+
n = 50
(h)
[7]Sm3+
n = 29
(i)
[8]Sm3+
n = 43
(j)
[8]Eu3+
n = 27
(k)
[8]Gd3+
n = 58
(l)
[8]Tb3+
n = 25
(m)
[8]Dy3+
n = 34
(n)
[8]Ho3+
n = 39
(o)
Frequency
Mean bond-length (Å)

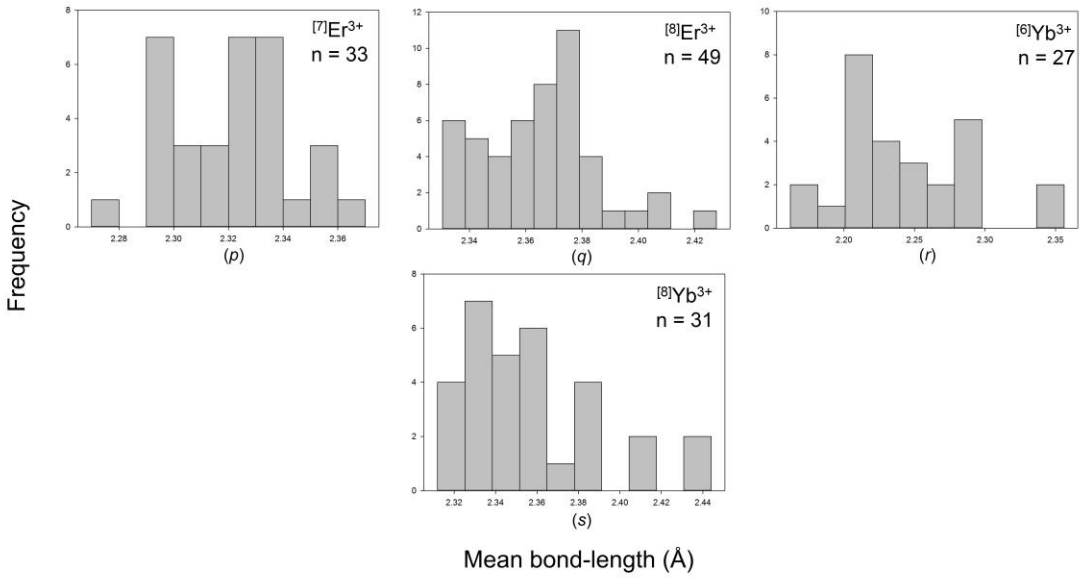

Figure 6 Mean bond-length distributions for selected configurations of the lanthanide ions bonded to O^{2-}: (*a*) $^{[8]}La^{3+}$, (*b*) $^{[9]}La^{3+}$, (*c*) $^{[9]}Ce^{3+}$, (*d*) $^{[8]}Pr^{3+}$, (*e*) $^{[9]}Pr^{3+}$, (*f*) $^{[7]}Nd^{3+}$, (*g*) $^{[8]}Nd^{3+}$, (*h*) $^{[9]}Nd^{3+}$, (*i*) $^{[7]}Sm^{3+}$, (*j*) $^{[8]}Sm^{3+}$, (*k*) $^{[8]}Eu^{3+}$, (*l*) $^{[8]}Gd^{3+}$, (*m*) $^{[8]}Tb^{3+}$, (*n*) $^{[8]}Dy^{3+}$, (*o*) $^{[8]}Ho^{3+}$, (*p*) $^{[7]}Er^{3+}$, (*q*) $^{[8]}Er^{3+}$, (*r*) $^{[6]}Yb^{3+}$, (*s*) $^{[8]}Yb^{3+}$.

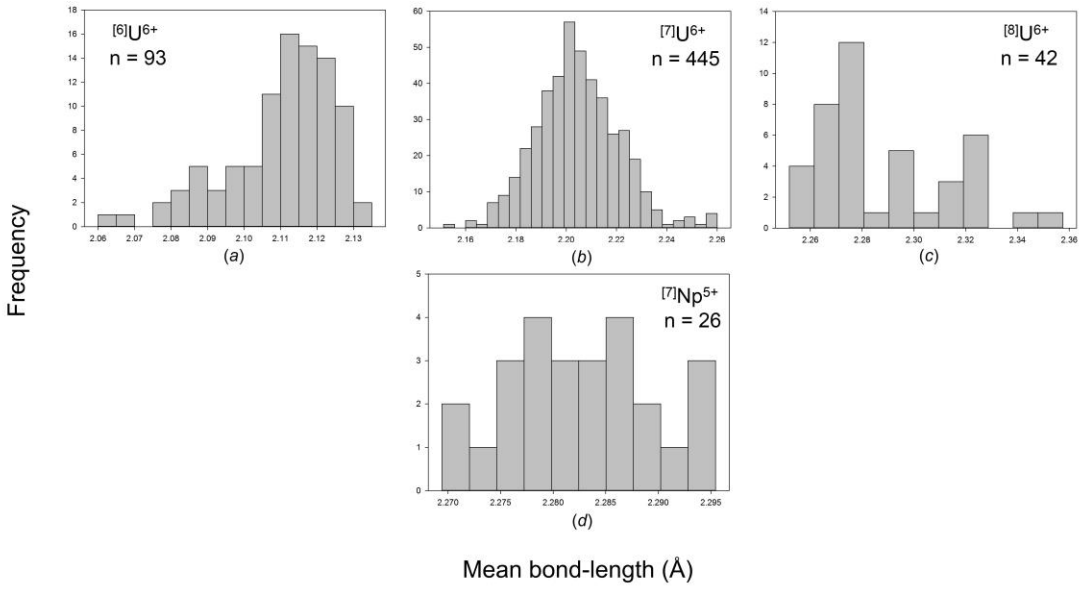

Figure 7 Mean bond-length distributions for selected configurations of the actinide ions bonded to O^{2-}: (*a*) $^{[6]}U^{6+}$, (*b*) $^{[7]}U^{6+}$, (*c*) $^{[8]}U^{6+}$, (*d*) $^{[7]}Np^{5+}$.

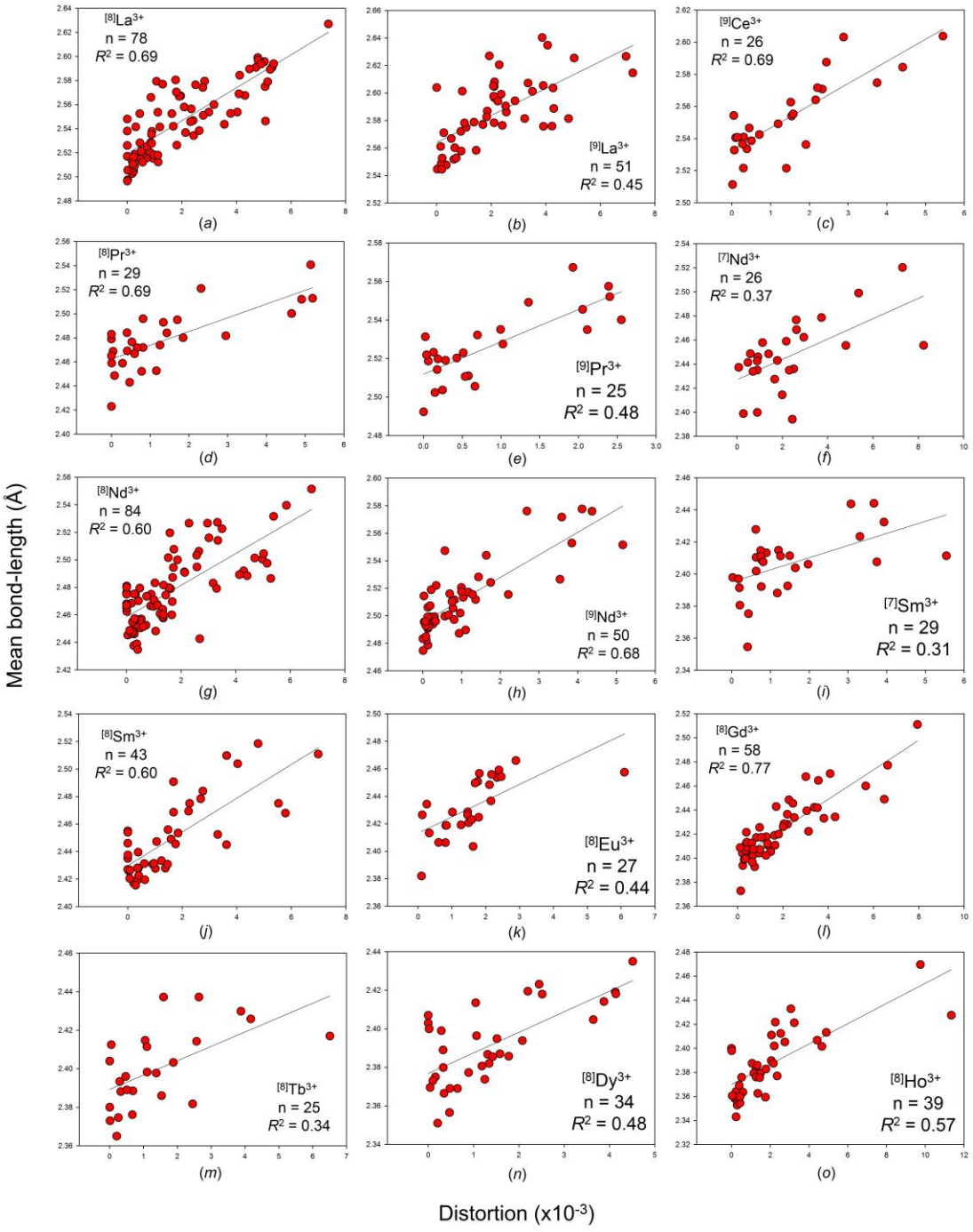
[8]La3+
n = 78
R2 = 0.69
(a)
[9]La3+
n = 51
R2 = 0.45
(b)
[9]Ce3+
n = 26
R2 = 0.69
(c)
[8]Pr3+
n = 29
R2 = 0.69
(d)
[9]Pr3+
n = 25
R2 = 0.48
(e)
[7]Nd3+
n = 26
R2 = 0.37
(f)
[8]Nd3+
n = 84
R2 = 0.60
(g)
[9]Nd3+
n = 50
R2 = 0.68
(h)
[7]Sm3+
n = 29
R2 = 0.31
(i)
[8]Sm3+
n = 43
R2 = 0.60
(j)
[8]Eu3+
n = 27
R2 = 0.44
(k)
[8]Gd3+
n = 58
R2 = 0.77
(l)
[8]Tb3+
n = 25
R2 = 0.34
(m)
[8]Dy3+
n = 34
R2 = 0.48
(n)
[8]Ho3+
n = 39
R2 = 0.57
(o)
Mean bond-length (Å)
Distortion (x10-3)

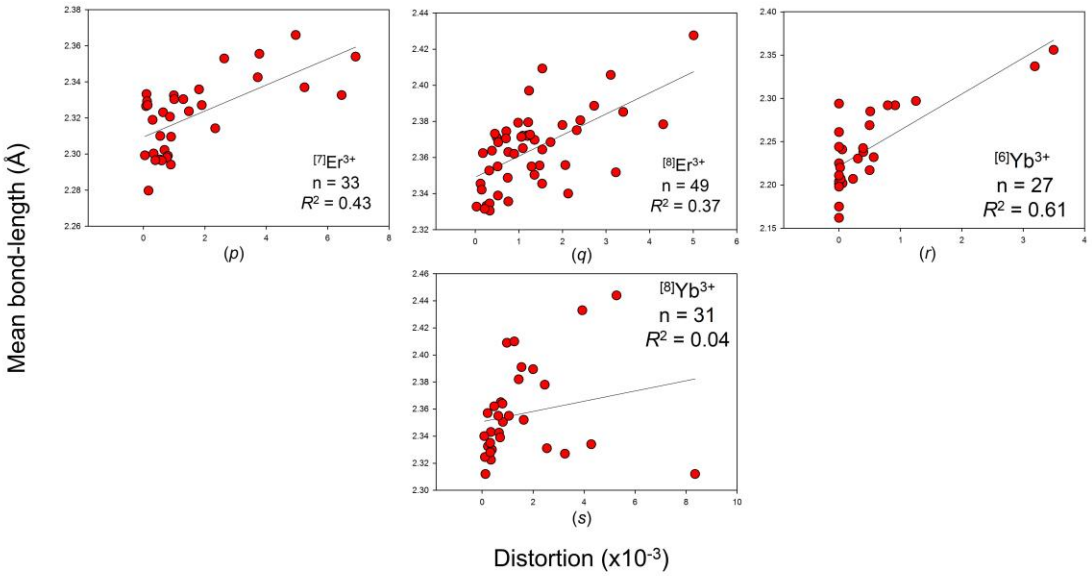

Figure 8 The effect of bond-length distortion on mean bond-length for selected configurations of the lanthanide ions bonded to O^{2-}: (*a*) $^{[8]}La^{3+}$, (*b*) $^{[9]}La^{3+}$, (*c*) $^{[9]}Ce^{3+}$, (*d*) $^{[8]}Pr^{3+}$, (*e*) $^{[9]}Pr^{3+}$, (*f*) $^{[7]}Nd^{3+}$, (*g*) $^{[8]}Nd^{3+}$, (*h*) $^{[9]}Nd^{3+}$, (*i*) $^{[7]}Sm^{3+}$, (*j*) $^{[8]}Sm^{3+}$, (*k*) $^{[8]}Eu^{3+}$, (*l*) $^{[8]}Gd^{3+}$, (*m*) $^{[8]}Tb^{3+}$, (*n*) $^{[8]}Dy^{3+}$, (*o*) $^{[8]}Ho^{3+}$, (*p*) $^{[7]}Er^{3+}$, (*q*) $^{[8]}Er^{3+}$, (*r*) $^{[6]}Yb^{3+}$, (*s*) $^{[8]}Yb^{3+}$.

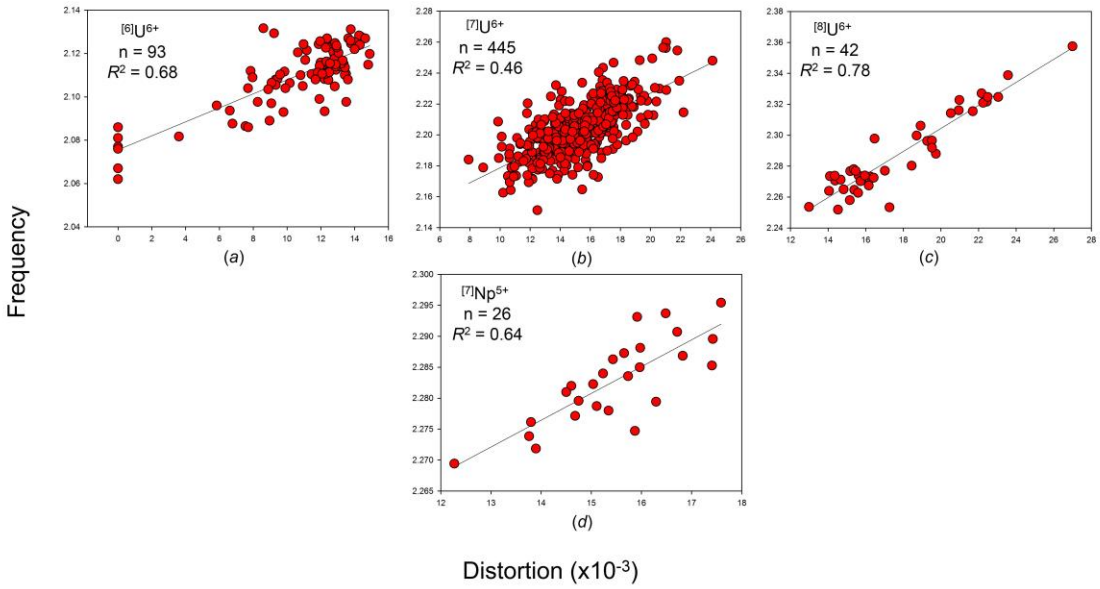

Figure 9 The effect of bond-length distortion on mean bond-length for selected configurations of the actinide ions bonded to O^{2-}: (*a*) $^{[6]}U^{6+}$, (*b*) $^{[7]}U^{6+}$, (*c*) $^{[8]}U^{6+}$, (*d*) $^{[7]}Np^{5+}$.

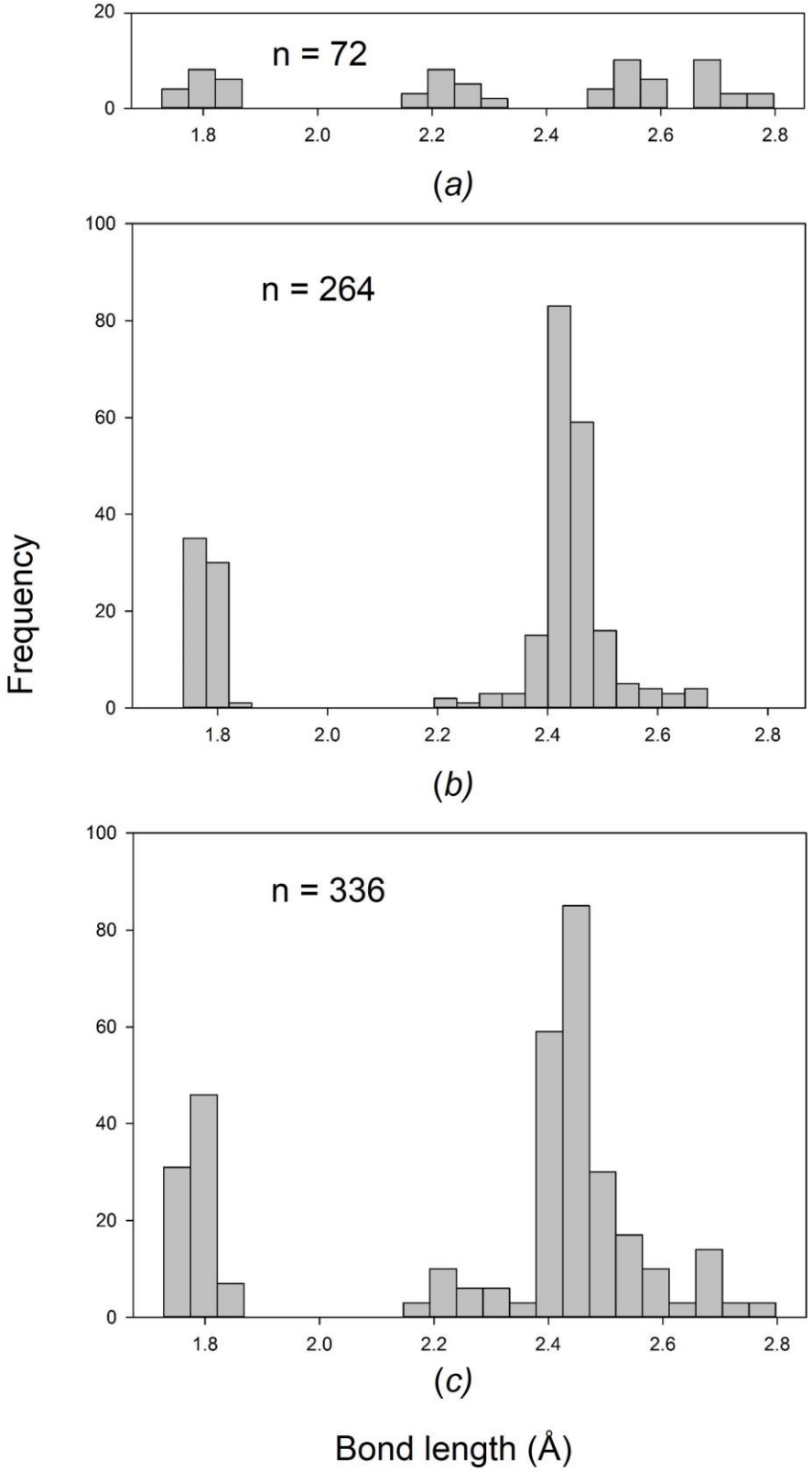

Figure 10 Bond-length distributions for (*a*) [2+2+4]-coordination, (*b*) [2+6]-coordination and (*c*) the aggregate of (*a*) and (*b*) for $U^{6+}O_8$ polyhedra**.**

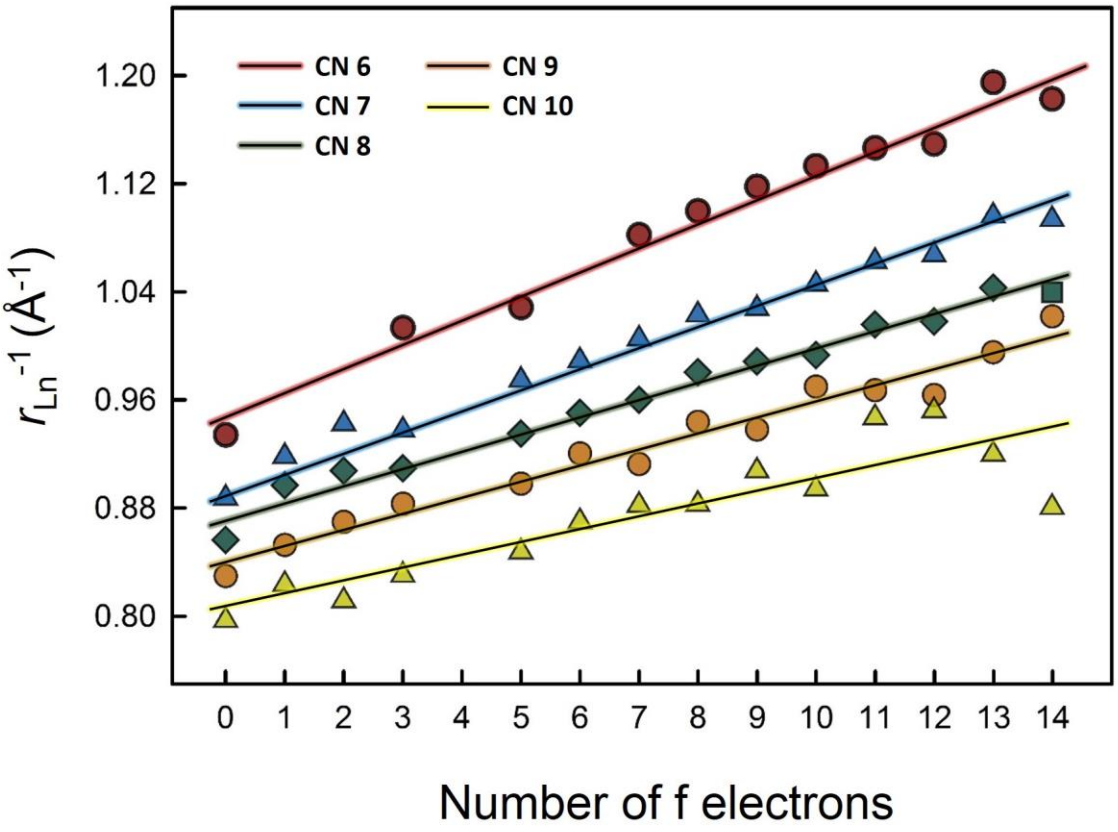

Figure 11 The lanthanide contraction as shown by the relation between the inverse of r_{Ln} as a function of the number of f electrons for Ln. Data are shown for coordination numbers 6 (red circles; R^2 = 0.979), 7 (blue triangles; R^2 = 0.988), 8 (green squares; R^2 = 0.982), 9 (orange circles; R^2 = 0.968) and 10 (yellow triangles; R^2 = 0.779). Solid lines are best-fit equations.

Table 1 Bond-length statistics for the lanthanide ions bonded to O^{2-}.

Ion	Coordination number	Number of bonds	Number of coordination polyhedra	Mean bond-length (Å)	Standard deviation (Å)	Range (Å)	Maximum bond-length (Å)	Minimum bond-length (Å)	Skewness	Kurtosis
La^{3+}	6	6	1	2.451	0.114	0.296	2.572	2.276	-	-
	7	126	18	2.507	0.112	0.501	2.825	2.324	0.7	0.0
	8	624	78	2.548	0.121	0.672	2.990	2.318	0.9	0.7
	9	459	51	2.586	0.124	0.641	2.977	2.336	0.8	0.6
	10	150	15	2.635	0.127	0.767	3.065	2.298	0.6	0.6
	11	11	1	2.661	0.108	0.348	2.875	2.527	-	-
	12	216	18	2.705	0.153	0.718	3.133	2.415	0.8	0.6
Ce^{3+}	7	14	2	2.469	0.063	0.258	2.620	2.362	-	-
	8	160	20	2.495	0.073	0.484	2.818	2.334	1.2	2.8
	9	234	26	2.553	0.101	0.619	2.916	2.297	0.8	1.8
	10	140	14	2.595	0.098	0.586	2.929	2.343	0.4	0.8
	11	33	3	2.686	0.202	0.898	3.155	2.257	-	-
	12	132	11	2.647	0.050	0.233	2.763	2.530	0.1	-0.5
Ce^{4+}	6	12	2	2.214	0.024	0.061	2.250	2.189	-	-
	8	104	13	2.345	0.075	0.468	2.640	2.172	1.0	2.9

	9	63	7	2.393	0.064	0.243	2.516	2.273	-	-
	10	20	2	2.436	0.125	0.607	2.652	2.045	-	-
	12	48	4	2.502	0.018	0.067	2.534	2.467	-	-
Pr^{3+}	7	42	6	2.441	0.099	0.496	2.777	2.281	-	-
	8	232	29	2.478	0.096	0.571	2.871	2.300	1.3	2.5
	9	225	25	2.526	0.077	0.524	2.864	2.340	1.0	2.6
	10	180	18	2.613	0.192	1.047	3.329	2.282	1.2	1.7
	11	22	2	2.688	0.257	0.912	3.218	2.306	-	-
	12	168	14	2.672	0.206	0.936	3.312	2.376	1.3	1.6
Nd^{3+}	6	96	16	2.365	0.042	0.265	2.559	2.294	2.1	7.7
	7	182	26	2.447	0.122	0.734	2.917	2.183	0.9	1.3
	8	672	84	2.478	0.105	0.625	2.891	2.266	0.9	1.0
	9	450	50	2.512	0.086	0.663	2.992	2.329	1.8	5.5
	10	80	8	2.585	0.153	0.597	2.937	2.340	-	-
	12	156	13	2.622	0.054	0.221	2.737	2.516	0.0	-0.8
Sm^{3+}	6	42	7	2.352	0.075	0.267	2.509	2.242	-	-
	7	203	29	2.406	0.094	0.513	2.761	2.248	1.1	1.8
	8	344	43	2.450	0.103	0.641	2.853	2.212	0.9	1.3
	9	72	8	2.494	0.095	0.582	2.864	2.282	-	-

	10	80	8	2.560	0.161	0.754	3.067	2.313	-	-
	12	24	2	2.714	0.285	0.843	3.159	2.316	-	-
Eu^{2+}	8	16	2	2.628	0.071	0.219	2.738	2.519	-	-
	9	9	1	2.693	0.111	0.308	2.841	2.533	-	-
Eu^{3+}	7	70	10	2.391	0.112	0.489	2.704	2.215	-	-
	8	216	27	2.432	0.100	0.603	2.859	2.256	0.6	0.5
	9	90	10	2.467	0.075	0.484	2.783	2.299	-	-
	10	20	2	2.530	0.147	0.524	2.829	2.305	-	-
Gd^{3+}	6	36	6	2.304	0.038	0.154	2.408	2.254	-	-
	7	133	19	2.375	0.088	0.483	2.707	2.224	1.4	3.0
	8	464	58	2.422	0.106	0.614	2.837	2.223	1.3	2.3
	9	135	15	2.476	0.114	0.644	2.928	2.284	1.3	2.1
	10	50	5	2.514	0.141	0.703	2.996	2.293	-	-
	11	11	1	2.627	0.196	0.768	3.061	2.293	-	-
Tb^{3+}	6	30	5	2.289	0.037	0.199	2.403	2.204	-	-
	7	42	6	2.358	0.117	0.444	2.676	2.232	-	-
	8	200	25	2.400	0.093	0.607	2.867	2.260	1.6	4.8
	9	72	8	2.440	0.070	0.328	2.614	2.286	-	-
	10	40	4	2.513	0.172	0.710	2.991	2.281	-	-

Tb^{4+}	6	42	7	2.181	0.049	0.213	2.324	2.111	-	-
Dy^{3+}	6	72	12	2.275	0.056	0.240	2.420	2.180	-	-
	7	119	17	2.353	0.105	0.561	2.748	2.187	1.3	2.2
	8	272	34	2.392	0.092	0.496	2.723	2.227	0.9	0.9
	9	27	3	2.446	0.091	0.355	2.652	2.297	-	-
	10	40	4	2.482	0.134	0.617	2.880	2.263	-	-
Ho^{3+}	6	90	15	2.263	0.047	0.213	2.385	2.172	-	-
	7	154	22	2.336	0.077	0.546	2.752	2.206	1.5	4.6
	8	312	39	2.387	0.111	0.714	2.936	2.222	1.5	3.7
	9	27	3	2.411	0.056	0.186	2.527	2.341	-	-
	10	20	2	2.499	0.185	0.683	2.935	2.252	-	-
Er^{3+}	6	48	8	2.252	0.025	0.113	2.310	2.197	-	-
	7	231	33	2.321	0.096	0.646	2.772	2.126	1.8	4.9
	8	392	49	2.364	0.088	0.577	2.734	2.157	1.0	1.4
	9	90	10	2.414	0.078	0.416	2.684	2.268	-	-
	10	20	2	2.436	0.031	0.102	2.492	2.390	-	-
Tm^{3+}	6	84	14	2.250	0.062	0.229	2.386	2.157	-	-
	7	56	8	2.317	0.121	0.499	2.651	2.152	-	-
	8	152	19	2.362	0.109	0.593	2.743	2.150	1.1	1.4

	9	18	2	2.418	0.093	0.393	2.625	2.232	-	-
	10	10	1	2.431	0.075	0.248	2.541	2.293	-	-
Yb^{3+}	6	162	27	2.217	0.043	0.215	2.356	2.141	0.9	1.0
	7	126	18	2.292	0.066	0.490	2.635	2.145	1.2	4.6
	8	248	31	2.339	0.086	0.582	2.710	2.128	1.1	2.9
	9	36	4	2.385	0.043	0.170	2.489	2.319	-	-
	10	20	2	2.468	0.158	0.613	2.852	2.239	-	-
Lu^{3+}	6	132	22	2.226	0.037	0.201	2.317	2.116	0.0	1.1
	7	63	9	2.295	0.076	0.483	2.614	2.131	-	-
	8	144	18	2.342	0.103	0.583	2.778	2.195	1.8	4.8
	9	27	3	2.359	0.065	0.244	2.476	2.232	-	-
	10	10	1	2.516	0.276	0.747	3.007	2.260	-	-

Table 2 Bond-length statistics for the actinide ions bonded to O^{2-}.

Ion	Coordination number	Number of bonds	Number of coordination polyhedra	Mean bond-length (Å)	Standard deviation (Å)	Range (Å)	Maximum bond-length (Å)	Minimum bond-length (Å)	Skewness	Kurtosis
Th^{4+}	8	96	12	2.418	0.071	0.444	2.691	2.247	1.1	2.5
	9	99	11	2.462	0.110	0.635	2.836	2.201	0.7	1.6
	10	10	1	2.505	0.040	0.108	2.560	2.452	-	-
	12	36	3	2.580	0.042	0.168	2.642	2.474	-	-
U^{4+}	7	14	2	2.318	0.103	0.434	2.514	2.080	-	-
	8	40	5	2.379	0.146	0.608	2.824	2.216	-	-
	9	9	1	2.427	0.091	0.325	2.604	2.279	-	-
	10	30	3	2.460	0.056	0.273	2.642	2.369	-	-
	12	84	7	2.501	0.021	0.086	2.545	2.459	-0.2	-0.8
U^{5+}	6	6	1	2.131	0.047	0.105	2.164	2.059	-	-
	7	21	3	2.250	0.160	0.476	2.538	2.062	-	-
U^{6+}	6	558	93	2.110	0.219	0.628	2.359	1.731	-0.7	-1.4
	7	3115	445	2.204	0.274	1.083	2.775	1.692	-0.7	-1.1
	8	336	42	2.288	0.307	1.069	2.797	1.728	-0.8	-0.8
Np^{5+}	6	6	1	2.211	0.259	0.550	2.395	1.845	-	-

	7	182	26	2.283	0.284	0.779	2.591	1.812	-0.9	-1.1
	8	32	4	2.369	0.317	0.945	2.770	1.825	-0.9	-0.8
Np^{6+}	7	42	6	2.189	0.285	0.760	2.486	1.726	-0.9	-1.1
	8	8	1	2.261	0.282	0.669	2.442	1.773	-	-
Np^{7+}	6	12	2	2.051	0.230	0.530	2.409	1.879	-	-
Am^{3+}	9	9	1	2.503	0.057	0.113	2.578	2.465	-	-
Cm^{3+}	9	9	1	2.490	0.056	0.111	2.564	2.453	-	-

Table 3 Mean bond-length statistics for the lanthanide ions bonded to O^{2-}.

Ion	Coordination number	Number of coordination polyhedra	Grand mean bond-length (Å)	Standard deviation (Å)	Mean bond-length range (Å)	Maximum mean bond-length (Å)	Minimum mean bond-length (Å)	Skewness	Kurtosis
La^{3+}	6	1	2.451	-	0.000	2.451	2.451	-	-
	7	18	2.507	0.024	0.090	2.556	2.466	-	-
	8	78	2.548	0.030	0.130	2.627	2.497	0.3	-0.8
	9	51	2.586	0.025	0.096	2.640	2.545	-	-
	10	15	2.635	0.024	0.097	2.697	2.600	-	-
	11	1	2.661	-	0.000	2.661	2.661	-	-
	12	18	2.705	0.037	0.110	2.765	2.655	-	-
Ce^{3+}	7	2	2.469	0.014	0.019	2.479	2.460	-	-
	8	20	2.495	0.023	0.081	2.549	2.469	-	-
	9	26	2.553	0.024	0.092	2.604	2.511	-	-
	10	14	2.595	0.018	0.068	2.650	2.582	-	-
	11	3	2.686	0.042	0.073	2.711	2.638	-	-
	12	11	2.647	0.016	0.061	2.689	2.628	-	-
Ce^{4+}	6	2	2.214	0.021	0.029	2.228	2.199	-	-

	8	13	2.345	0.014	0.045	2.366	2.321	-	-
	9	7	2.393	0.010	0.027	2.406	2.379	-	-
	10	2	2.436	0.027	0.039	2.455	2.416	-	-
	12	4	2.502	0.010	0.023	2.512	2.490	-	-
Pr^{3+}	7	6	2.441	0.012	0.034	2.459	2.425	-	-
	8	29	2.478	0.024	0.118	2.541	2.423	-	-
	9	25	2.526	0.018	0.075	2.567	2.492	-	-
	10	18	2.613	0.043	0.127	2.684	2.557	-	-
	11	2	2.688	0.039	0.056	2.716	2.660	-	-
	12	14	2.672	0.058	0.180	2.801	2.621	-	-
Nd^{3+}	6	16	2.365	0.022	0.087	2.408	2.321	-	-
	7	26	2.447	0.029	0.126	2.520	2.394	-	-
	8	84	2.478	0.026	0.117	2.552	2.435	0.7	0.0
	9	50	2.512	0.026	0.103	2.578	2.475	-	-
	10	8	2.585	0.048	0.116	2.655	2.539	-	-
	12	13	2.622	0.020	0.067	2.662	2.596	-	-
Sm^{3+}	6	7	2.352	0.025	0.060	2.371	2.311	-	-
	7	29	2.406	0.019	0.090	2.444	2.355	-	-
	8	43	2.450	0.028	0.103	2.519	2.416	-	-

	9	8	2.494	0.023	0.069	2.533	2.463	-	-
	10	8	2.560	0.031	0.106	2.623	2.516	-	-
	12	2	2.714	0.058	0.082	2.755	2.673	-	-
Eu^{2+}	8	2	2.628	0.006	0.008	2.632	2.624	-	-
	9	1	2.693	-	0.000	2.693	2.693	-	-
Eu^{3+}	7	10	2.391	0.020	0.066	2.414	2.348	-	-
	8	27	2.432	0.021	0.084	2.466	2.382	-	-
	9	10	2.467	0.027	0.091	2.532	2.440	-	-
	10	2	2.530	0.004	0.005	2.532	2.527	-	-
Gd^{3+}	6	6	2.304	0.027	0.071	2.338	2.267	-	-
	7	19	2.375	0.021	0.074	2.410	2.335	-	-
	8	58	2.422	0.025	0.138	2.511	2.373	-	-
	9	15	2.476	0.028	0.097	2.531	2.435	-	-
	10	5	2.514	0.025	0.053	2.539	2.486	-	-
	11	1	2.627	-	0.000	2.627	2.627	-	-
Tb^{3+}	6	5	2.289	0.022	0.050	2.313	2.263	-	-
	7	6	2.358	0.025	0.064	2.388	2.323	-	-
	8	25	2.400	0.020	0.072	2.437	2.365	-	-
	9	8	2.440	0.009	0.022	2.448	2.426	-	-

	10	4	2.513	0.033	0.082	2.553	2.471	-	-
Tb^{4+}	6	7	2.181	0.011	0.028	2.196	2.168	-	-
Dy^{3+}	6	12	2.275	0.025	0.075	2.320	2.244	-	-
	7	17	2.353	0.017	0.061	2.378	2.316	-	-
	8	34	2.392	0.021	0.084	2.435	2.351	-	-
	9	3	2.446	0.017	0.029	2.465	2.437	-	-
	10	4	2.482	0.025	0.049	2.504	2.454	-	-
Ho^{3+}	6	15	2.263	0.018	0.053	2.288	2.235	-	-
	7	22	2.336	0.013	0.051	2.356	2.305	-	-
	8	39	2.387	0.027	0.127	2.470	2.343	-	-
	9	3	2.411	0.021	0.038	2.425	2.387	-	-
	10	2	2.499	0.002	0.003	2.500	2.497	-	-
Er^{3+}	6	8	2.252	0.021	0.061	2.274	2.213	-	-
	7	33	2.321	0.021	0.086	2.366	2.280	-	-
	8	49	2.364	0.021	0.097	2.428	2.331	-	-
	9	10	2.414	0.018	0.059	2.450	2.391	-	-
	10	2	2.436	0.006	0.008	2.441	2.432	-	-
Tm^{3+}	6	14	2.250	0.023	0.068	2.281	2.213	-	-
	7	8	2.317	0.020	0.058	2.346	2.288	-	-

	8	19	2.362	0.022	0.078	2.403	2.325	-	-
	9	2	2.418	0.016	0.023	2.429	2.407	-	-
	10	1	2.430	-	0.000	2.430	2.430	-	-
Yb^{3+}	6	27	2.242	0.047	0.194	2.356	2.162	-	-
	7	18	2.325	0.026	0.108	2.378	2.270	-	-
	8	31	2.356	0.034	0.132	2.444	2.312	-	-
	9	4	2.385	0.017	0.039	2.410	2.371	-	-
	10	2	2.421	0.038	0.054	2.447	2.394	-	-
Lu^{3+}	6	22	2.226	0.022	0.083	2.250	2.167	-	-
	7	9	2.295	0.023	0.070	2.331	2.261	-	-
	8	18	2.342	0.024	0.085	2.385	2.301	-	-
	9	3	2.359	0.005	0.008	2.364	2.356	-	-
	10	1	2.516	-	0.000	2.516	2.516	-	-

Table 4 Mean bond-length statistics for the actinide ions bonded to O^{2-}.

Ion	Coordination number	Number of coordination polyhedra	Grand mean bond-length (Å)	Standard deviation (Å)	Mean bond-length range (Å)	Maximum mean bond-length (Å)	Minimum mean bond-length (Å)	Skewness	Kurtosis
Th^{4+}	8	12	2.425	0.018	0.052	2.456	2.403	-	-
	9	11	2.462	0.013	0.038	2.485	2.447	-	-
	10	1	2.505	-	0.000	2.505	2.505	-	-
	12	3	2.580	0.030	0.058	2.614	2.556	-	-
U^{4+}	7	2	2.318	0.020	0.029	2.332	2.304	-	-
	8	5	2.379	0.025	0.067	2.417	2.350	-	-
	9	1	2.427	-	0.000	2.427	2.427	-	-
	10	3	2.460	0.007	0.013	2.467	2.454	-	-
	12	7	2.501	0.008	0.024	2.514	2.489	-	-
U^{5+}	6	1	2.131	-	0.000	2.131	2.131	-	-
	7	3	2.250	0.002	0.003	2.251	2.248	-	-
U^{6+}	6	93	2.110	0.015	0.070	2.132	2.062	-1.1	0.9
	7	445	2.204	0.017	0.109	2.260	2.151	0.3	0.6
	8	42	2.288	0.026	0.106	2.358	2.252	-	-

Np^{5+}	6	1	2.211	-	0.000	2.211	2.211	-	-
	7	26	2.283	0.007	0.026	2.295	2.269	-	-
	8	4	2.369	0.014	0.031	2.384	2.353	-	-
Np^{6+}	7	6	2.189	0.011	0.031	2.204	2.173	-	-
	8	1	2.261	-	0.000	2.261	2.261	-	-
Np^{7+}	6	2	2.048	0.021	0.030	2.063	2.033	-	-
Am^{3+}	9	1	2.503	-	0.000	2.503	2.503	-	-
Cm^{3+}	9	1	2.490	-	0.000	2.490	2.490	-	-

Acknowledgements This work was funded by a PGS-D3 Scholarship from the Natural Sciences and Engineering Research Council of Canada and by a UM Duff Roblin and GETS Fellowship from the University of Manitoba to OCG.

References

Allen, F. H., Kennard, O., Watson, D. G., Brammer, L., Orpen, A. G. & Taylor, R. (1987). J. Chem. Soc., Perkin Trans. 2, S1-S19.

Allmann, R. (1975). Monatsh. Chem. 106, 779-793.

Bagus, P. S., Lee, Y. S. & Pitzer, K. S. (1975). Chem. Phys. Lett. 33, 408-411.

Brese, N. E. & O'Keeffe, M. (1991). Acta Cryst. B47, 192-197.

Brown, I. D. (1978). Chem. Soc. Rev. 7, 359-376.

Brown, I. D. & Altermatt, D. (1985). Acta Cryst. B41, 244-247.

Brown, I. D. & Shannon, R. D. (1973). Acta Cryst. A29, 266-282.

Burns, P. C., Ewing, R. C., Hawthorne, F. C. (1997). Can. Mineral. 35, 1551-1570.

Choppin, G. R. (2002). J. Alloys Compd. 344, 55–59.

Cooper, M. A. & Hawthorne, F. C. (2001). Can. Mineral. 39, 797-807.

Craw, J. S., Vincent, M. A., Hillier, I. H. & Wallwork, A. L. (1995). J. Phys. Chem. 99, 10181-10185.

Denning, R. G. (2007). J. Phys. Chem. A 111, 4125-4143.

Gagné, O. C. & Hawthorne, F. C. (2015). Acta Cryst. B71, 562-578.

Gagné, O. C. & Hawthorne, F. C. (2016). Acta Cryst. B72, 602-625.

Gagné, O. C. & Hawthorne, F. C. (2017a). Bond-length distributions for ions bonded to oxygen: Results for the non-metals and discussion of lone-pair stereoactivity and the polymerization of PO_4. In review (Acta Cryst. B).

Gagné, O. C. & Hawthorne, F. C. (2017b). Bond-length distributions for ions bonded to oxygen: Metalloids and poor metals. In review (Acta Cryst. B).

Gagné, O. C. & Hawthorne, F. C. (2017c). Mean bond-length variations in crystals for ions bonded to oxygen. In review (Acta Cryst. B).

Ginderow, D. & Cesbron, F. (1985). Acta Cryst. C41, 654-657.

Goldschmidt, V. M., Barth, T. & Lunde, G. (1925). Geochemische Verteilungsgesetze der Elemente. V. Isomorphie und Polymorphie der Sesquioxyde. Die Lanthaniden-Kontraktion und ihre Konsequenzen. Skrifter Norske Videnskaps —Akad. Oslo, (I) Mat. Natur. Kl. No. 7.

Grigor'ev, M. S., Gulev, B. F. & Krot, N. N. (1986). Radiokhimiya 28, 690-694.

Grigor'ev, M. S., Baturin, N. A., Tananaev, I. G. & Krot, N. N. (1993) Radiokhimiya 35, 12-16.

Hayton, T. W. (2010). Dalton Trans. 39, 1145–1158.

Küchle, W., Dolg, M. & Stoll, H. (1997). J. Phys. Chem. A 101, 7128-7133.

Jubera, V., Gravereau, P., Chaminade, J.-P. & Fouassier, C. (2001). J. Solid State Chem. 156, 161-167.

Locock, A. J. & Burns, P. C. (2003a). Can. Mineral. 41, 91-101.

Locock, A. J. & Burns, P. C. (2003b). Mineral. Mag. 67, 1109-1120.

Maron, L. & Eisenstein, O. (2000). J. Phys. Chem. A104, 7140-7143.

Mayer, J. M. (1988). Inorg. Chem. 27, 3899-3903.

Neidig, M. L., Clark, D. L. & Martin, R. L. (2013). Coord. Chem. Rev. 257, 394– 406.

Orpen, A. G., Brammer, L., Allen, F. H., Kennard, O., Watson, D. G. & Taylor, R. (1989). J. Chem. Soc., Dalton Trans., S1-S83.

Piret, P. & Piret-Meunier, J. (1988). Bull Minéral. 111, 439-442.

Pyykkö, P. (1988). Relativistic effects in structural chemistry. Chem. Rev. 88, 563-594.

Quadrelli, E. A. (2002). Lanthanide contraction over the 4f series follows a quadratic decay. Inorg. Chem. 41, 167-169.

Raymond, K. N., Wellman, D. L., Sgarlata, C. & Hill, A. P. (2010). Curvature of the lanthanide contraction: an explanation. C. R. Chim 13, 849-852.

Seitz, M., Oliver, A. G. & Raymond, K.N. (2007). J. Am. Chem. Soc. 129, 11153-11160.

Seth, M., Dolg, M. Fulde, P. & Schwerdtfeger, P. (1995). J. Am. Chem. Soc. 117, 6597-6598.

Shannon, R. D. (1976). Acta Cryst. A32, 751–767.

Slater, J. C. (1930). Phys. Rev. 36, 57–64.

Urusov, V. S. (2003). Z. Kristallogr. 218, 709-719.